

A *Herschel* Survey of Cold Dust in Disks Around Brown Dwarfs and Low-Mass Stars*

Paul M. Harvey¹, Thomas Henning², Yao Liu^{3,4}, François Ménard⁵, Christophe Pinte⁵, Sebastian Wolf³, Lucas A. Cieza⁶, Neal J. Evans II¹, Ilaria Pascucci⁷

ABSTRACT

We report the complete photometric results from our *Herschel* study which is the first comprehensive program to search for far-infrared emission from cold dust around young brown dwarfs. We surveyed 50 fields containing 51 known or suspected brown dwarfs and very low mass stars that have evidence of circumstellar disks based on *Spitzer* photometry and/or spectroscopy. The objects with known spectral types range from M3 to M9.5. Four of the candidates were subsequently identified as extragalactic objects. Of the remaining 47 we have successfully detected 36 at $70\mu\text{m}$ and 14 at $160\mu\text{m}$ with S/N greater than 3, as well as several additional possible detections with low S/N. The objects exhibit a range of [24]–[70] micron colors suggesting a range in mass and/or structure of the outer disk. We present modeling of the spectral energy distributions of the sample and discuss trends visible in the data. Using two Monte Carlo radiative transfer codes we investigate disk masses and geometry. We find a very wide

¹Astronomy Department, University of Texas at Austin, 1 University Station C1400, Austin, TX 78712-0259; pmh@astro.as.utexas.edu, nje@astro.as.utexas.edu

²Max Planck Institut for Astronomy, Königstuhl 17, 69117 Heidelberg, Germany;henning@mpia.de

³University of Kiel, Institute of Theoretical Physics and Astrophysics, Leibnizstr. 15, 24098 Kiel, Germany; wolf@astrophysik.uni-kiel.de, yliu@pmo.ac.cn

⁴Graduate School of the Chinese Academy of Sciences, Beijing 100080, China; yliu@pmo.ac.cn

⁵UJF-Grenoble 1/CNRS-INSU, Institut de Planétologie et d'Astrophysique (IPAG) UMR 5274, BP 53, 38041 Grenoble cedex 9, France; menard@obs.ujf-grenoble.fr, christophe.pinte@obs.ujf-grenoble.fr

⁶Institute for Astronomy, University of Hawaii, 2680 Woodlawn Dr., Honolulu, HI 96822; lcieza@ifa.hawaii.edu, Sagan Fellow

⁷Lunar and Planetary Laboratory, Department of Planetary Sciences, University of Arizona, 1629 E. University Blvd., Tucson, AZ 85721; pascucci@lpl.arizona.edu

range in modeled total disk masses from less than $10^{-6} M_{\odot}$ up to $10^{-3} M_{\odot}$ with a median disk mass of order $3 \times 10^{-5} M_{\odot}$, suggesting that the median ratio of disk mass to central object mass may be lower than for T Tauri stars. The disk scale heights and flaring angles, however, cover a range consistent with those seen around T Tauri stars. The host clouds in which the young brown dwarfs and low-mass stars are located span a range in estimated age from ~ 1 – 3 Myr to ~ 10 Myr and represent a variety of star-forming environments. No obvious dependence on cloud location or age is seen in the disk properties, though the statistical significance of this conclusion is not strong.

Subject headings: protoplanetary disks — stars: formation — brown dwarfs

1. Introduction

The existence of circumstellar disks around low-mass stars and substellar objects is now a well-established phenomenon. Many of the observations of the lowest mass objects have taken advantage of the *Spitzer Space Telescope's* (Werner et al. 2004) exquisite sensitivity in the $3 - 24\mu\text{m}$ spectral region, e.g. Allers et al. (2006); Hernandez et al. (2007); Guieu et al. (2007); Luhman et al. (2005) (and many of the other references in Table 3) to find thermal emission above that expected from the photospheres of these objects. With the likely surface density gradient of such disks, however, most of the dust is typically located at radii too large to emit strongly at those *Spitzer* wavelengths, particularly for low-luminosity substellar objects. At longer wavelengths, $70 - 1000\mu\text{m}$, few disks have been detected around brown dwarfs, e.g. (Klein et al. 2003; Scholz, Jayawardhana & Wood 2006; Bouy et al. 2008; Riaz & Gizis 2008). In addition to being more sensitive to the total disk mass, observations at the longer wavelengths are also sensitive to the disk scale height, dust settling, and degree of flaring. The relationship between disk mass and structure and planet formation is highly uncertain, but nominally one might expect objects with lower mass disks to form planetary systems with lower average mass planets (Mordasini et al. 2012). Below some disk mass limit, though, there may be too little material for any planet formation, so understanding disks around the lowest mass objects will place important constraints on likely planet formation around them.

**Herschel* is an ESA space observatory with science instruments provided by European-led Principal Investigator consortia and with important participation from NASA.

The relatively small number of detections of disks around very low-mass stars and brown dwarfs beyond the range of *Spitzer's* $24\mu\text{m}$ MIPS band and its IRS instrument, has made it difficult to investigate the properties and evolution of the cool dust component of these disks where most of the mass is located. We describe here the results from a *Herschel* GT1 (Guaranteed Time, Phase 1) program that obtained 70 and $160\mu\text{m}$ photometry of a statistically significant number of confirmed or candidate brown dwarfs and low-mass stars close to the sub-stellar limit. Our early results on the first three objects observed are described by Harvey et al. (2012) (hereafter, Paper I). In the following sections we describe the observed sample, the details of the observing parameters and data reduction, the overall properties of the spectral energy distributions (SED's), and extensive radiative transfer modeling of the SED's to extract physical properties of the disks. We conclude with a discussion of the overall results from this study based on the complete sample together with existing data in the literature on cold dust in young brown dwarf and T Tauri disks. The most important goals of this program were to use the *Herschel* far-ir photometry to place useful limits on the outer disk properties around brown dwarfs, in particular, the mass and disk geometry. We also aimed at providing as complete as possible SED coverage for future characterization at longer wavelengths with the Atacama Large Millimeter Array (ALMA).

2. The Sample

Our sample of 50 targets was chosen from the literature to include young objects at or below the sub-stellar limit in the nearby regions of star formation listed in Table 1. Both confirmed and candidate BD's were included. Table 1 lists rough ages for each of the clouds based on the range of measurements in the literature. Although there are often more precise numbers quoted for median cloud ages in the literature, the age spreads observed around the median have led us to consider only two age bins in our sample, the clouds with ages ≤ 5 Myr and those with ages of order 10 Myr. Because the sub-stellar limit is only roughly defined as a function of spectral type and age, we included objects generally with spectral types later than M5 with the exception of several in the range M3 – M4.8. The most important additional selection criterion was evidence for circumstellar dust emission, likely a disk, as shown by $8\text{--}24\mu\text{m}$ excess emission over the photosphere. Our goal was to reach flux limits at $70\mu\text{m}$ low enough that we would be likely to detect disk emission based on the shorter wavelength *Spitzer* data or to set useful upper limits. Our sample was specifically trimmed to not include objects that might be bright enough to be detected in *Herschel's* large scale shallow surveys of star-forming regions (André et al. 2010). The selection process involved “predicting” the $70\mu\text{m}$ flux density based on the $8\text{--}24\mu\text{m}$ color and $24\mu\text{m}$ brightness using typical SED's for brighter young T Tauri stars as a guide. As might be expected, the final

results showed our rough “predictions” to be accurate to only \pm a factor of 3. An additional selection criterion was an attempt to select objects that did not lie in regions of strong, structured diffuse emission as based on *Spitzer* 24 and $70\mu\text{m}$ images when available. Even with this criterion, one object, CFHTWIR96, was completely hidden in much brighter diffuse emission at both observed wavelengths, and a number of sources were invisible at $160\mu\text{m}$ against the Galactic background/foreground.

Because the sample included candidate BD’s, a few objects included in the observed sample have turned out not to be stellar or sub-stellar objects with disks, including four found to be extragalactic and one that may be at an earlier evolutionary state with a substantial envelope or extragalactic (ChaJ11080397-7730382). The four extragalactic objects include 2MASSJ16080175-3912316 and IRACJ16084679-3902074 from the study by Allen et al. (2007) and found to be extragalactic by Comerón, Spezzi & López Martí (2009) and Comerón (2011). The source 2MASSJ1129140-7546256 was found by Luhman & Muench (2008) to exhibit emission lines characteristic of a galaxy. The object 2MASSJ16084747-3905087 from Allen et al. (2007) has been found to consist of two nearby objects, one of which peaks in the near-ir and the other at longer wavelengths by Luhman (private comm.). This is most obvious in the *Spitzer* IRAC band 1 ($3.6\mu\text{m}$) image where the object is clearly double, consistent with it being a blend between a star and extragalactic object.

Table 3 lists the complete sample of low-mass stars and brown dwarfs, including one object, ISO143 that was included serendipitously in the field of ISO138 and which lies at the boundary between stellar and sub-stellar objects. With the inclusion of this object and the removal of the four extra-galactic sources, the final sample consists of 46 likely or confirmed BD’s/low mass stars with circumstellar disk emission, and one object, ChaJ11080397-7730382 (hereafter cha110804), classified as a “possible Class 1 source” by Luhman et al. (2008). We include this latter source because its *Spitzer* IRAC band 4 ($8.0\mu\text{m}$) image shows faint nebulosity around the object that is at least consistent with it being a Galactic source. We have also measured upper limits to its 1.6 and $2.2\mu\text{m}$ fluxes from the 2MASS images of the area, since it was listed as undetected by the survey. Figures 1 and 2 display the physical properties of the observed sample graphically. Figure 1 shows a plot of the observed total luminosities ($1\text{--}160\mu\text{m}$) versus spectral type for the 43 objects with published spectral types assuming the distances listed in Table 1. This figure and several later figures show individual points with symbols for each host cloud; in addition, the two oldest clouds, Upper Sco and TWA, are indicated with red symbols to highlight any possible age-dependent trends using the two age bins discussed above. Figure 1 illustrates graphically the wide range in luminosities present in our sample. It is also clear that there is a substantial range in luminosity at any given spectral type and likewise a range in spectral types at any given luminosity. There is no obvious correlation with cloud age for either of these distributions. Figure 2

shows histograms of the observed total luminosities of all the objects and the distribution of spectral types for the 43 objects with published types; the separate contributions from each host cloud to the total sample are indicated, illustrating the range of luminosity and spectral type present in the sample from each host cloud.

Because of the various features of the above selection process, our study is not useful to estimate disk frequencies for young brown dwarfs. The sample, however, is useful to compare the frequencies of cold dust emission relative to warmer dust emission due to, for example, differences in outer disk mass or structure in the outer disk. More generally, our far-ir photometry has the potential to provide the first statistically meaningful sample of disk masses around BD’s. Since we have objects from various star-forming regions covering a range in estimated ages from $\sim 1\text{--}3$ Myr to $\sim 8\text{--}10$ Myr, this sample may also be useful for investigating disk evolution around BD’s, e.g. mass and geometry. We discuss all of these issues more fully in §6.

3. Observations and Data Reduction

Our program, GT1_pharve01_2, was designed to take advantage of the excellent sensitivity and spatial sampling of the PACS photometer (Poglitsch et al. 2010) on *Herschel* (Pilbratt et al. 2010). All the observations were made using exactly the same mode with essentially the same total integration time. We utilized the PACS “mini-scan-map” mode which images simultaneously at 70 and $160\mu\text{m}$ and uses two separate scan maps at an angle of 40° for good 1/f noise reduction. This mode provides high and relatively uniform sensitivity over an area of order $60''\times 90''$ in the center (within 80% of peak coverage). Table 2 lists the relevant parameters for all the observations reported here. The OBSID’s for all the observations are listed in Table 3. The 1σ noise levels for the combined OBSID’s for each object were expected to be ~ 1 mJy at $70\mu\text{m}$ and 2.3 mJy at $160\mu\text{m}$ according to the *Herschel* observation-planning tool HSPOT which is based on standard aperture photometry estimates. In fact, we achieved 10–20% better noise levels at $70\mu\text{m}$ probably because of our use of psf-fitting photometry instead of aperture photometry. The uncertainties at $160\mu\text{m}$ were almost entirely set by the level of diffuse emission present in the images, which differed widely between objects.

The data were first processed with the Herschel Interactive Processing Environment, HIPE version 7.3, with a script that utilizes standard high-pass filtering for point-source observations, and which processes the two separate OBSID’s for each object together. The portions of scan legs where the telescope was stopped or not scanning at a uniform velocity were not used for this processing. The output of this script consists of *fits* files of the image,

coverage, and uncertainty. The uncertainty images are not yet reliable at this stage in the *Herschel* mission, so we estimated uncertainties in additional ways described below.

The next stage of data reduction utilized the psf-fitting photometry tool, *c2dphot*, originally developed by the *c2d Spitzer* Legacy Team (Harvey et al. 2006; Evans et al. 2007), and based on the earlier DOPHOT tool (Schechter, Mateo, & Saha 1993). This tool can be used in various modes, including finding peaks above the background and fitting a psf to the local maxima, or fitting a psf to any fixed position in the image. This latter mode is especially useful for estimating the noise and determining upper limits. The noise levels quoted for our sources were determined this way by fitting a grid of nine positions on and around the BD position within the high-coverage area. Upper limits were also estimated this way as well as by inserting artificial stars into the images, particularly for the $160\mu\text{m}$ data. We also computed aperture fluxes for comparison with the psf-fitted values, and those values agree well. In addition, we have computed aperture-flux “curves-of-growth” to be sure that there are no systematic problems with the psf-fit photometry. At $160\mu\text{m}$ most of the images were contaminated substantially by structured, diffuse emission that dominated the flux uncertainties.

4. Observational Results

Figures 3–7 (electronic version only) show images of all 47 of the observed low mass young objects. A summary of our measured flux densities is given in Table 3. We have not included the four objects found to be extragalactic, but do list the object cha110804 described as “possible Class 1” by Luhman et al. (2008) since its luminosity is probably in the same range as the other objects. The entries in Table 3 given as upper limits have been determined by finding the maximum brightness source that could have been present at the position of the object without us reliably detecting it; therefore, these should be viewed as firm limits, equivalent to $\sim 3\sigma$. For objects where an examination of the image showed a possible detection, we report the formal flux level derived from the psf-fit and the uncertainty determined as described above using multiple psf-fit positions in blank parts of the image.

All of the objects in Table 3 have been observed over a wide range of wavelengths by some or all of the 2MASS (Skrutskie et al. 2006) and DENIS surveys, the recent WISE survey (Wright et al. 2010), numerous *Spitzer* programs using IRAC and MIPS, as well as 36 with the IRS instrument on *Spitzer*. This enables us to present very complete SED’s for all the sources, and as discussed below, enables model fitting to derive limits on physical parameters of the circumstellar disks. We show these in two forms. Figure 8 shows the SED’s of all the objects superposed and normalized to the $1.6\mu\text{m}$ flux density (or upper limit in

the case of cha110804). Figures 9 – 12 show the individual SED’s for all the objects except cha110804.

Figure 8 shows that the observed SED’s between 1 and $100\mu\text{m}$ differ considerably, and it suggests also that there appears to be a relatively continuous distribution of slopes in the mid- to far-infrared. We can also illustrate this conclusion with the color-color diagram in Figure 13 that shows a plot of the ratio of νF_ν at $24\mu\text{m}$ versus $70\mu\text{m}$ compared to the comparable ratio at $3.6\mu\text{m}$ versus $24\mu\text{m}$. This also shows a relatively continuous distribution of colors, although 90% of the objects have $\nu F_\nu(24\mu\text{m}) \geq \nu F_\nu(70\mu\text{m})$. The very red object cha110804 is clearly beyond the end of the distribution of the other objects that are believed to have circumstellar disks but not substantial envelopes.

One question we can consider with just this simplified analysis of the SED’s is whether there is any evidence for differences in disks with age or environment. The symbols for each object in Figure 13 have been coded to denote the host cloud in which they are found. Within the relatively small number statistics for some of the regions, there is no clear trend in far-ir excess as a function of the location/age of the cloud in which each object is found. The same conclusions holds if we restrict the sample to a subset of objects with well-determined spectral types in the M5–6 range which has a reasonable number of sources.

5. Radiative Transfer Modeling

In Paper I we showed results from modeling the disks around the first three objects observed in this program, 2MASS120733, ISO138, and SSSPM110209. Despite the degeneracy inherent in such modeling, we found that for those three cases with excellent SED coverage we were able to constrain the circum-object disk masses and geometry to some degree. For this current study we performed radiative transfer modeling of the complete set of objects, though the results are probably most useful for those with the most complete SED coverage. We have not tried extensively to fit the Spitzer IRS data in the area of the silicate feature which is generally viewed as arising in the disk atmospheres, e.g. Oloffson et al. (2009), and we have assumed a single, uniform grain composition.

We used the two radiative transfer codes discussed already in Paper I, MC3D described by Wolf, Henning & Stecklum (1999); Wolf (2003) and MCFOST described by Pinte et al. (2006, 2009). Both codes are three-dimensional, radiative transfer codes using the Monte-Carlo method. NextGen stellar atmosphere models (Hauschildt, Allard & Baron 1999; Allard & Hauschildt 1995) were used for the stellar input to the disk models with the photospheric temperature set by the assumed spectral type where available. With each code we modeled

each SED with a parametric disk. We use a dust density distribution with a Gaussian vertical profile $\rho(r, z) = \rho_0(r) \exp(-z^2/2h^2(r))$, valid for a vertically isothermal, hydrostatic, non self-gravitating disk. We use power-law distributions for the dust surface density $\Sigma(r) = \Sigma_0 (r/r_0)^{-p}$ and the scale height $h(r) = h_0 (r/r_0)^\gamma$ where r is the radial coordinate in the equatorial plane. The parameter h_0 is the scale height at a fiducial radius chosen to be $r_0 = 100$ AU for easier comparison with previous BD and T Tauri disk models. The scale height parameters, γ and h_0 , are free parameters in the modeling and not calculated from assumptions of hydrostatic equilibrium. The disk extends from an inner radius r_{in} to an outer limit radius r_{out} . The central star is represented by a sphere radiating uniformly.

We consider homogeneous spherical grains and we use the dielectric constants of astro-silicates (Draine 2003). The differential grain size distribution is given by $dn(a) \propto a^{-3.5} da$ with grain sizes between $a_{\text{min}} = 0.03\mu\text{m}$ and $a_{\text{max}} = 1\mu\text{m}$ or 1mm . The mean grain density is 3.5 g cm^{-3} . Dust extinction and scattering opacities, scattering phase functions and Mueller matrices are calculated using Mie theory. The grain properties are taken to be independent of position within the disk. All disk masses discussed below are described as “Total” disk mass of gas and dust together. We make no assumptions about the gas distribution in the disk, but we assume a ratio of 100 for gas mass relative to dust mass for comparison with other disk mass estimates. Of course the SED modeling is only sensitive to the dust mass, and even in that case only to dust up to some nominal size of a few times the longest observed wavelength. In principle, the two radiative transfer codes should give the same result, but because of differences in the exact model grid, there were sometimes modest differences. For example, the MCFOST grid in mass was spaced by 0.5 in $\log_{10}(\text{Mass})$ from $10^{-6} - 10^{-2} M_\odot$ (total disk mass), while the MC3D grid was spaced by 1.0 in $\log_{10}(\text{Mass})$ from $5 \times 10^{-8} - 5 \times 10^{-4} M_\odot$.

As discussed in Paper I, the choice of outer radius for the disks makes essentially no difference to the model SED in the spectral range of our study because most of the far-ir emission comes from dust at radii inside of 20 AU; so this was left fixed in all the models at 100 AU. The choice of outer radius also makes only a small difference in the probable values of most other disk parameters. This is shown both in Paper I by a comparison of the disk parameters for 2MASS120733 for outer radii of of 75 versus 25 AU, and by the modeling described by Bouy et al. (2008) for 2MASS04442713. For example, the total disk mass is driven largely by the total far-infrared/submm flux (see also discussion below and Figure 16).

Because of the remaining degeneracy in the model-fitting despite our extended SED coverage, we present the results largely from the Bayesian probability analysis for various disk parameters. In other words, at this point in the model-fitting it is not appropriate to choose

a “best-fit” model or model parameter(s) but simply to state the most probable range for disk parameters. For example, sometimes the model with the absolutely lowest chi-squared implies a parameter value somewhat offset from the peak of its probability distribution, since the probability distribution for each parameter is marginalized over all possible values of the remaining parameters. This can lead to noticeable differences between some of the disk parameters for two models that fit the SED nearly equally well.

The overall results of the modeling are displayed in several figures. Figures 9–12 show example model SED’s from the set that produces reasonable fits for each object. Figure 14 shows histograms of the total of the probability distributions for all the program objects as well as the subset detected at $160\mu\text{m}$ to show the likely average distribution of these parameters. Figure 15 shows the distribution of the most probable disk masses as a function of spectral type for the 43 objects with published spectral types, and finally Figure 16 shows the distribution of probable disk masses versus the 70 and $160\mu\text{m}$ luminosities for each object. We discuss these results below. More refined modeling of individual sources will be pursued in a subsequent study where we will report individual disk parameters.

In Paper I we discussed the comparison between our model results for the first three objects and several existing models in the literature for those objects. To our knowledge only two additional objects from our sample, CFHT Tau 9 and OTS 44, have a published model. In a recent study Riaz et al. (2012a) investigated the radial dependence of grain composition in brown dwarfs relative to T Tauri stars. Since they used a geometrical model of the disk similar to those in our study, it is possible to compare the resulting model fits directly. In particular, for CFHT Tau 9 without the additional spectral coverage of *Herschel*, they found an inner disk radius equal to the sublimation radius, a disk inclination of order $30\text{--}40^\circ$, and a flaring index of 1.1 provide a good fit to the overall SED. These values are essentially identical to the probability peaks in our fits for this object. Luhman et al. (2005) have modeled the disk around OTS44, but their model was based on different disk parameters making it difficult to perform a detailed comparison. Finally, Riaz et al. (2012b) have recently reported a large submm flux in the *Herschel* SPIRE bands from 2M1207 that would imply a much larger disk mass than found from our modeling, but have since retracted that conclusion (Riaz et al. 2012c).

6. Discussion

6.1. Overview of Modeling Results

Despite the inherent degeneracies in SED modeling without angular size information, there are several conclusions that appear relatively firm as illustrated in the figures described above. The majority of the disks are best modeled with scale heights h_o at the fiducial radius of 100 AU of order 5 – 20 AU and radial scale height dependences γ in the range 1.1 – 1.2. Their inner radii are likely close to the dust sublimation radii which are typically of order 5×10^{-3} AU for the faintest objects up to $\sim 1.5 \times 10^{-2}$ AU for the most luminous. Their surface density gradients are best fit with a relatively shallow slope of $p \sim 0.5 - 1.0$ ($\Sigma \propto r^{-p}$) although this value is not well constrained. There is clearly a very wide range in likely masses with a median value of order $3 \times 10^{-5} M_{\odot}$ ($0.03 M_{Jup}$), a value which is roughly the same for both the objects with spectral types later than M6 and earlier than M6. Unless these masses are severely underestimated due to grain growth to sizes well beyond a value to which this study is sensitive, this suggests that future giant planet formation would be very difficult in these disks. If we assume that spectral type is a rough proxy for brown dwarf mass, then Figure 15 suggests that the ratio of disk mass to sub-stellar mass covers quite a wide range, of order a few $\times 10^{-5}$ up to $\sim 10^{-2}$.

It is well understood that the mass of circumstellar disks is best measured at submm or mm wavelengths where the disks are optically thin except in the very central regions and the dust is virtually all emitting on the Rayleigh-Jeans part of its SED. The longest wavelength observed in our study is $160\mu\text{m}$. Although the optical depth in the plane of all our model disks is well above unity at $160\mu\text{m}$, Figure 17 shows that for most of the objects which are naturally not observed edge-on, the disks are vertically optically thin in emission over radial distances where more than half the total flux is emitted. This figure also shows that the situation at $70\mu\text{m}$ is more problematic with only $\sim 1/3$ of the total flux emitted outside the $\tau = 1$ radius. This implies that the $160\mu\text{m}$ flux may be an approximate measure of disk mass, limited mainly by its relative insensitivity to very cool and very large dust grains and by the fact that $160\mu\text{m}$ is not completely into the Rayleigh-Jeans part of the dust emission spectrum. Figure 16 illustrates this possibility by comparing the most probable model disk masses to the observed 70 and $160\mu\text{m}$ luminosities. With the exception of the two outliers, both the TWA objects, there does appear to be a reasonably good correlation between $160\mu\text{m}$ flux and likely disk mass, as well as even with $70\mu\text{m}$ luminosity. No such correlation exists between the total luminosity, for example, and $160\mu\text{m}$ flux. Even though our $160\mu\text{m}$ data already provide good disk mass estimates, further observations of all these objects with ALMA will be extremely important to determine both the disk fluxes at (sub)mm wavelengths and disk sizes.

6.2. Host Cloud Correlations?

The 46 low-mass objects with disks in our study are located in various star-forming clouds as listed in Table 1. These host clouds have a range of estimated ages as well as other less quantifiable differences. For example, the TW Hydra Association is a very low stellar-density group, while some of the younger regions have a much higher density of young stars and brown dwarfs in their core. In any case, a number of figures in our study that distinguish between these host clouds display no clear correlation of any observed or modeled parameter with the location of the objects. We have also investigated a simple grouping of objects into two bins, those in clouds with estimated ages of order 10 Myr, TWA and Upper Sco, and the remainder that are significantly younger. Even with this division which encompasses 13 objects in the “older” group, we find no significant differences in disk properties. The median probable disk mass in the “older” group is $\log_{10}M_{disk} = -5.0 \pm 0.85 M_{\odot}$ while the median for the younger group is $\log_{10}M_{disk} = -4.5 \pm 1.05 M_{\odot}$.

6.3. Comparison With Young Stellar Objects

In Paper I we made an initial comparison of the disk properties of our first three program objects with young stars that will eventually burn hydrogen, the T Tauri stars. Because such stars are brighter than brown dwarfs, there exists a large quantity of observations and modeling in the literature to characterize their disks via dust emission, scattering, and even gas emission. The recent review by Williams & Cieza (2011) summarizes the state of understanding of disks around T Tauri stars. The disk geometries for such stars are quite similar to the geometries found to be likely fits to the disks around our sample of very low mass objects within the mutual uncertainties. The typical surface density gradient we found of $\Sigma \propto r^{-0.5}$ to $r^{-1.0}$ and typical scale height and flaring mentioned above are certainly well within the range for models of solar-mass young objects. It is interesting, though, that if the disk vertical structure is determined solely by hydrostatic equilibrium with well-mixed gas and dust, lower central object masses would lead to more flared disks around brown dwarfs than around T Tauri stars (Walker et al. 2004) which is not obvious in our results. This has already been noted by Szűcs et al. (2010) in a comparison of median SED’s between BD’s and T Tauri stars. The most significant clear difference between our sample of sub-stellar objects and T Tauri stars is the total disk mass inferred from modeling and submm/mm observations. Disk masses around T Tauri stars are commonly found to be in the range of $10^{-3} - 10^{-1} M_{\odot}$, well above our median disk mass of $3 \times 10^{-5} M_{\odot}$. The most massive disks in our sample are comparable to the masses of a few previously modeled brown dwarfs (e.g. Bouy et al. 2008)) and to the low end of the distribution of disks around T Tauri stars. The

masses of our sample objects are uncertain, but assuming a median mass $\sim few \times 10^{-2} M_{\odot}$ for the brown dwarfs, the median ratio of disk mass to central object mass may be a factor of 3–10 lower than for T Tauri stars. When the results from the shallow large scale *Herschel* surveys are available, it will be interesting to re-examine this conclusion with the inclusion of brighter brown dwarfs.

7. Summary

We have used *Herschel/PACS* to observe nearly 50 young sub-stellar and nearly sub-stellar objects with likely circum“stellar” disks implied by previous *Spitzer* data, and we have increased the number of such objects that are detected beyond $24\mu\text{m}$ by a factor of ~ 5 . We find a wide range in ratios of far-ir to mid-ir flux. Preliminary modeling of the disks to fit the observed SED’s shows that the dust disk geometries are similar to those of their higher mass counterparts, but the range of masses extends well below the masses of disks around T Tauri stars, i.e. down below $10^{-6} M_{\odot}$. This implies that for most of the objects, unless giant planets have already formed, there is not nearly enough mass to form them. Our radiative transfer modeling shows that *Herschel’s* $160\mu\text{m}$ band is already long enough to provide reasonable disk mass estimates. Although our sample selection precludes drawing conclusions about disk frequencies, we have found no clear dependence of disk mass or geometry on the age of the star-forming region where the object is located.

8. Acknowledgments

We thank the referee, K. Luhman, for bringing to our attention several spectral type determinations that we missed and pointing out two of the extragalactic interlopers in our sample. Support for this work, as part of the NASA *Herschel* Science Center data analysis funding program, was provided by NASA through a contract issued by the Jet Propulsion Laboratory, California Institute of Technology to the University of Texas. LAC was supported by NASA through the Sagan Fellowship Program. FM and CP acknowledge support from ANR (contracts ANR-07-BLAN-0221 and ANR-2010-JCJC-0504-01), the European Commission’s 7th Framework Program (contract PERG06-GA-2009-256513) and Programme National de Physique Stellaire (PNPS) of CNRS/INSU, France. SW acknowledges support by the German Research Foundation (contract FOR 759). YL acknowledges support by the German Academic Exchange Service.

This publication makes use of data products from the Wide-field Infrared Survey Ex-

plorer, which is a joint project of the University of California, Los Angeles, and the Jet Propulsion Laboratory/California Institute of Technology, funded by the National Aeronautics and Space Administration.

The DENIS project has been partly funded by the SCIENCE and the HCM plans of the European Commission under grants CT920791 and CT940627. It is supported by INSU, MEN and CNRS in France, by the State of Baden-Württemberg in Germany, by DGICYT in Spain, by CNR in Italy, by FFwFBWF in Austria, by FAPESP in Brazil, by OTKA grants F-4239 and F-013990 in Hungary, and by the ESO C&EE grant A-04-046. Jean Claude Renault from IAP was the Project manager. Observations were carried out thanks to the contribution of numerous students and young scientists from all involved institutes, under the supervision of P. Fouqué, survey astronomer resident in Chile.

Table 1: Location of Observed Young Brown Dwarfs

Cloud	Number of BD's	Assumed Distance	Assumed Age	References
Ophiuchus	3	125 pc	1–3 Myr	1
Taurus	4	140 pc	1–3 Myr	2
Chamaeleon I	12	160 pc	1–3 Myr	3
Chamaeleon II	3	178 pc	1–3 Myr	1
Lup I	1	150 pc	1–3 Myr	1
Lup III	5	200 pc	~5 Myr	4
Sigma Ori	7	360 pc	~3 Myr	5
Upper Sco	11	145 pc	~11 Myr	6
TWA	2	54 pc	8–10 Myr	7

References. — (1) As adopted by *Spitzer c2d*, Evans et al. 2007; (2) Kenyon, Gómez & Whitney 2008; (3) Luhman 2008; (4) Comerón, F. 2008, 2009; (5) Caballero et al. 2007; (6) Pecaute, Mamajek & Bubar 2012; (7) Webb et al. 1999

Table 2: Observational Parameters

Parameter	Value	Comments
OBSID Type	PACS Mini-Scan-Map	Two Crossed OBSID's
Wavelengths	$70\mu\text{m}$, $160\mu\text{m}$	
Number of Scan Legs	8	
Scan Length	$3'$	
Cross Scan Step	$4''$	
Scan Angles	70° , 110°	Relative to Detector
Repetitions	7	Per OBSID
Peak Intg Time Per Pixel	504 sec	Per OBSID

Table 3. Source Summary (Program ID = GT1_pharve01_2)

Object	RA/Dec Center (J2000)				OBSID's	Obs. Date	F_ν 70 μ m mJy	F_ν 160 μ m mJy	Sp. Type	Refs ^a
	h	m	s	° ' "						
CFHT-Tau9	04	24	26.5	+26 49 51	1342227059/60	2011-08-22	9.5 ± 1.2	< 6	M6.2	14
KPNO-Tau6	04	30	07.2	+26 08 21	1342227011/2	2011-08-21	2.3 ± 1.0	< 5	M9.0	14,15
KPNO-Tau7	04	30	57.2	+25 56 40	1342227999/8000	2011-09-04	3.5 ± 1.0	< 7	M8.2	14
CFHT-Tau12	04	33	09.5	+22 46 49	1342227013/4	2011-08-21	1.5 ± 0.7	< 8	M6.5	14,15
SOri053825	05	38	25.4	-02 42 41	1342226721/2	2011-08-17	2.0 ± 1.1	< 7	M7.0	7,5,6
SOri053834	05	38	33.9	-02 45 08	1342226723/4	2011-08-18	7.4 ± 0.9	10.1 ± 5.0	M4.0	33,5,6
SOri053848	05	38	48.2	-02 44 01	1342226725/6	2011-08-18	2.7 ± 1.0	< 4		5,6
SOri053855	05	38	55.4	-02 41 21	1342226727/8	2011-08-18	1.9 ± 1.0	< 5	M5.0	8,5
SOri053902	05	39	02.0	-02 35 01	1342228431/2	2011-09-07	27.9 ± 4.5	20.0 ± 4.0	M2-4	8,5,6
SOri36	05	39	26.9	-02 36 56	1342228429/30	2011-09-07	1.5 ± 0.8	< 5		5,6
SOri054004	05	40	04.5	-02 36 42	1342228363/4	2011-09-09	<1.2	< 3		5,6
SSSPM110209	11	02	09.8	-34 30 36	1342221849/50	2011-05-29	9.4 ± 0.6	8.6 ± 1.8	M8.5	30,13,32
2MJ110703	11	07	03.7	-77 24 31	1342223480/1	2011-06-23	24.6 ± 1.2	50.1 ± 12.0	M7.5	18,13,18,19
ChaHa9	11	07	19.2	-77 32 52	1342223482/3	2011-06-23	12.2 ± 0.8	<10	M5.5	22,13,21,23
Cha110804	11	08	04.0	-77 30 38	1342223484/5	2011-06-23	94.4 ± 1.6	84.1 ± 8.0		13,18
ISO138	11	08	19.0	-77 30 41	1342218699/700	2011-04-16	3.4 ± 0.8	<15	M6.5	23,13,18,21
ISO143	11	08	22.3	-77 30 28	1342218699/700	2011-04-16	13.3 ± 0.9	10.2 ± 2.0	M5.0	23,13,21,22
ChaHa6	11	08	40.2	-77 34 17	1342223486/7	2011-06-34	14.4 ± 1.0	<10	M5.8	22,13,23
T37	11	08	50.9	-76 25 14	1342223468/9	2011-06-22	2.9 ± 0.9	< 3	M5.2	23,13,22
ISO165	11	08	55.0	-76 32 41	1342223470/1	2011-06-22	42.5 ± 0.8	30.0 ± 10.0	M5.5	23,13,18,21
Cha726	11	09	52.2	-76 39 13	1342223474/5	2011-06-23	10.4 ± 1.3	<30	M6.2	22,13,21,23
OTS44	11	10	11.4	-76 32 13	1342223472/3	2011-06-22	7.0 ± 1.0	<10	M9.5	24
ISO252	11	10	41.4	-77 20 48	1342223478/9	2011-06-23	8.7 ± 0.7	<10	M6.0	23,13,18,21
2MJ111145	11	11	45.3	-76 36 50	1342223476/7	2011-06-23	3.0 ± 1.0	<10	M8.0	20,13,18,21
2MJ120733	12	07	33.4	-39 32 54	1342202557/8	2010-08-10	7.1 ± 0.7	< 7	M8.0	31,13,27,29

Table 3—Continued

Object	RA/Dec Center (J2000)			OBSID's	Obs. Date	F_ν 70 μ m mJy	F_ν 160 μ m mJy	Sp. Type	Refs ^a			
	h	m	s							°	'	"
Allers-2	12	58	06.7	−77	09	09	1342224206/7	2011-07-14	3.4 ± 0.7	< 3	M6.0	2,1
Allers-6	13	07	18.0	−77	40	53	1342224202/3	2011-07-14	6.4 ± 0.9	<12	M5.0	2,1
Allers-7	13	08	27.2	−77	43	24	1342224204/5	2011-07-14	6.0 ± 0.9	< 7	M6.0	2,1
Allers-19	15	44	57.9	−34	23	39	1342226701/2	2011-08-17	2.2 ± 0.8	< 8	M4.5	2,1
usd155556	15	55	56.0	−20	45	18	1342227138/9	2011-08-23	12.2 ± 0.7	12.0 ± 2.5	M6.5	26,4,25
usd155601	15	56	01.0	−23	38	08	1342227132/3	2011-08-23	6.5 ± 0.8	11.4 ± 2.1	M6.5	26,4,25
usco128	15	59	11.2	−23	37	59	1342227134/5	2011-08-23	5.3 ± 0.7	4.1 ± 1.2	M7.0	28,4,25
usco112	16	00	26.6	−20	56	32	1342227140/1	2011-08-23	1.6 ± 0.8	< 7	M5.5	28,4,25
usco55	16	02	45.6	−23	04	50	1342227136/7	2011-08-23	11.1 ± 0.9	6.0 ± 1.2	M5.5	28,4,25
DENIS1603	16	03	34.7	−18	29	30	1342227831/2	2011-09-03	1.6 ± 0.9	< 5	M5.5	3,4
usd160603	16	06	03.9	−20	56	45	1342227142/3	2011-08-23	3.2 ± 1.0	3.8 ± 3.3	M7.5	26,4,25
2MJ160737	16	07	37.7	−39	21	39	1342227813/4	2011-09-02	14.4 ± 0.9	13.2 ± 8.5	M5.8	9,11
2MJ160814	16	08	15.0	−38	57	14	1342227825/6	2011-09-03	66.8 ± 1.5	49.0 ± 9.0	M4.8	9,11
IRACJ160828	16	08	28.1	−39	13	09	1342227817/8	2011-09-02	5.5 ± 1.0	< 7	M5.0	12,9,13,16
2MJ160859	16	08	59.5	−38	56	28	1342227823/4	2011-09-03	7.4 ± 0.9	11.8 ± 5.0	M8.0	9,11
usd160958	16	09	58.5	−23	45	19	1342227146/7	2011-08-23	4.1 ± 0.7	< 4	M6.5	26,4,25
usd161005	16	10	05.4	−19	19	36	1342227829/30	2011-09-03	4.3 ± 0.8	7.5 ± 1.5	M7.0	26,4,25
usd161833	16	18	33.2	−25	17	50	1342227827/8	2011-09-03	9.0 ± 1.5	12.0 ± 7.0	M6.0	26,4,25
usd161939	16	19	39.8	−21	45	35	1342227835/6	2011-09-03	15.3 ± 0.6	4.8 ± 3.0	M7.0	26,4,25
Allers-8	16	21	42.0	−23	13	43	1342227837/8	2011-09-03	34.3 ± 0.9	41.5 ± 11.0	M3.0	2,1
Allers-13	16	22	45.0	−23	17	13	1342227839/40	2011-09-03	12.0 ± 3.5	<15	M6.0	2,1
CFHTWIR96	16	27	40.8	−24	29	01	1342227841/2	2011-09-03	5.0 ± 20	130 ± 200	M8.2	17

Table 3—Continued

Object	RA/Dec Center (J2000)	OBSID's	Obs. Date	F_ν 70 μ m	F_ν 160 μ m	Sp. Type	Refs ^a
	h m s ° ' "			mJy	mJy		

^aFirst reference listed is for spectral type if measured; additional references are for various $\lambda < 40\mu$ m photometry

References. — (1) Allers et al. 2006; (2) Gully-Santiago, Allers & Jaffe 2012; (3) Bouy et al. 2007; (4) Wright et al. 2010 (WISE); (5) Caballero et al. 2007; (6) Hernandez et al. 2007; (7) Rigliaco et al. 2011; (8) Caballero et al. 2008; (9) Allen et al. 2007; (10) Comerón 2011; (11) Comerón, Spezzi & López Martí 2009; (12) López Martí, Eislöffel & Mundt 2005; (13) Skrutskie et al. (2MASS) 2006; (14) Guieu et al. 2007; (15) Rebull et al. 2010; (16) Mérim et al. 2008; (17) Alves de Oliveira et al. 2010; (18) Luhman et al. 2008; (19) Luhman & Muench 2008; (20) Luhman 2007; (21) López Martí et al. 2004; (22) Damjanov et al. 2007; (23) Luhman et al. 2004; (24) Luhman et al. 2005; (25) Scholz et al. 2007; (26) Martín, Delfosse & Guieu 2004; (27) DENIS; (28) Ardila, Martín & Basri 2000; (29) Riaz, Gizis & Hmiel 2006; (30) Scholz et al. 2005; (31) Gizis 2002; (32) Luhman et al. 2010; (33) Cody & Hillenbrand 2011

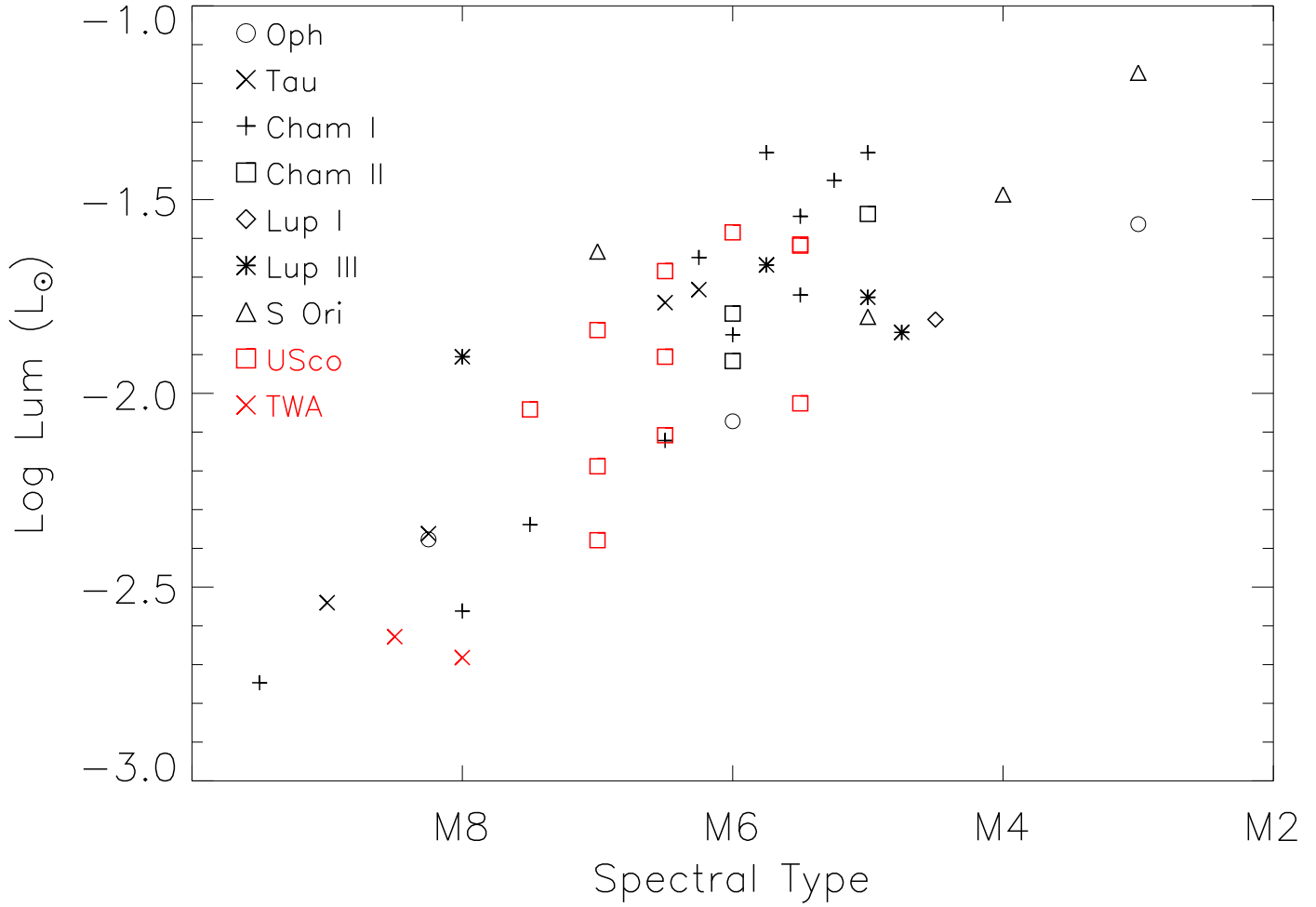


Fig. 1.— Observed luminosities versus spectral types for the 43 objects with determined spectral types in the literature. The symbols are color coded so that the two star-forming regions that are significantly older than the others, U Sco and TWA, are in red.

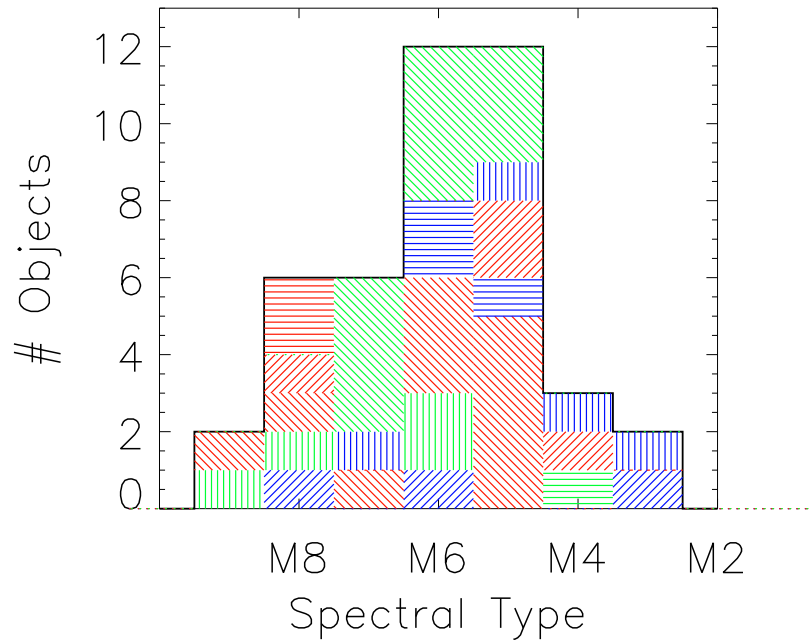
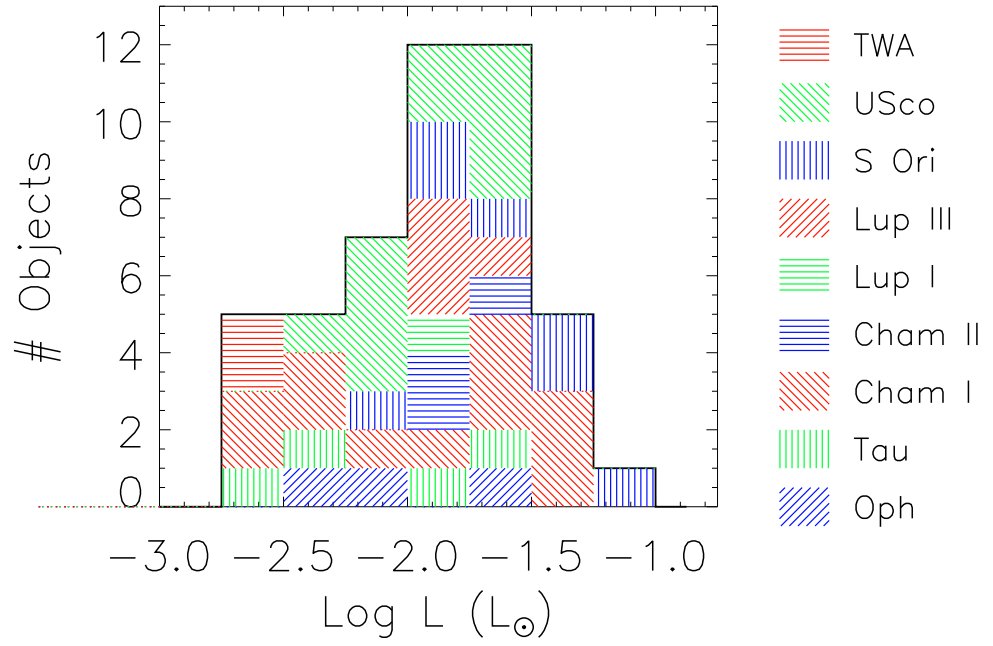


Fig. 2.— Histogram of observed luminosities ($1-200\mu\text{m}$) for all 47 objects and histogram of spectral types for the 43 objects with determined spectral types.

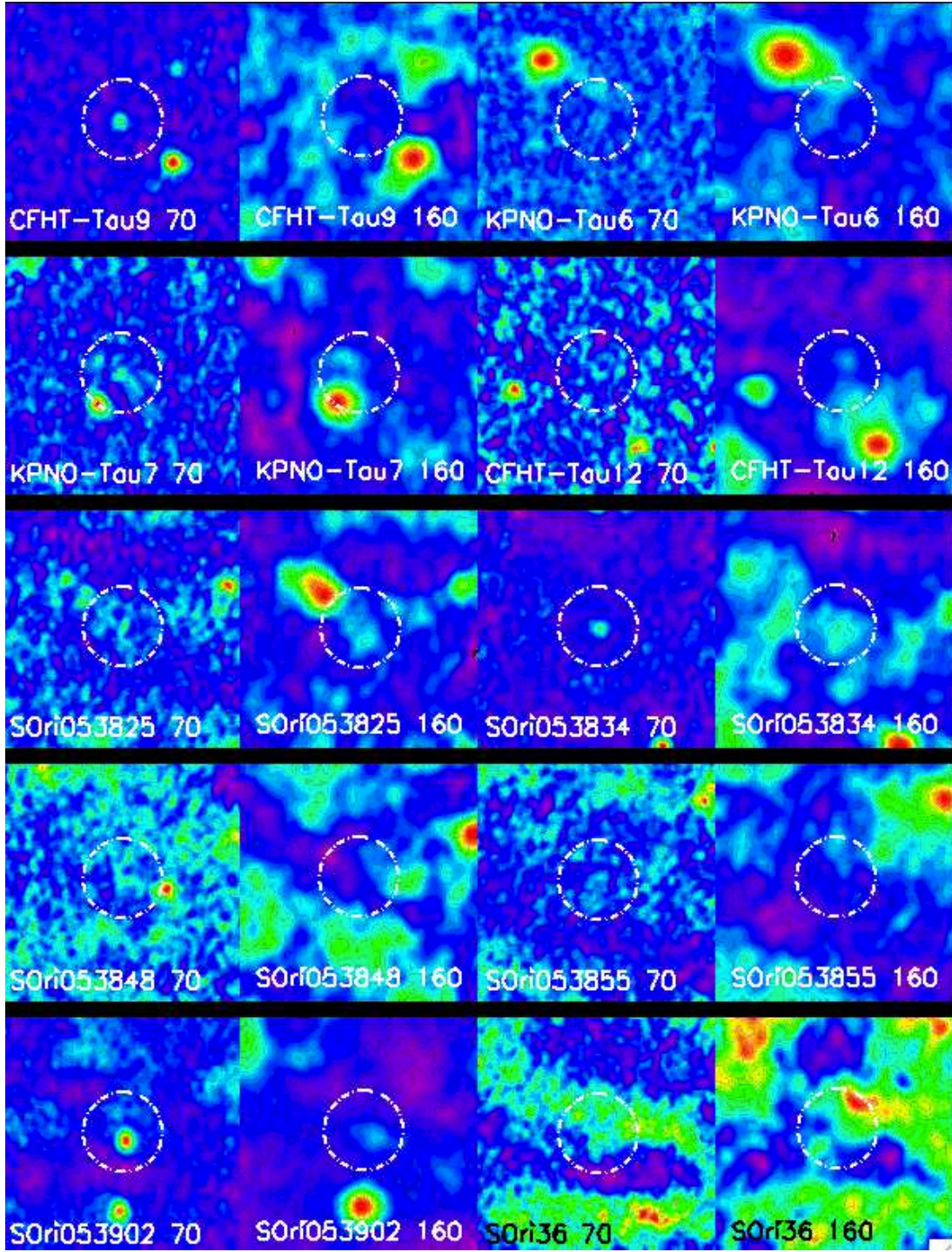


Fig. 3.— Images of first 10 objects in Table 3. Dotted circle is 30'' in diameter.

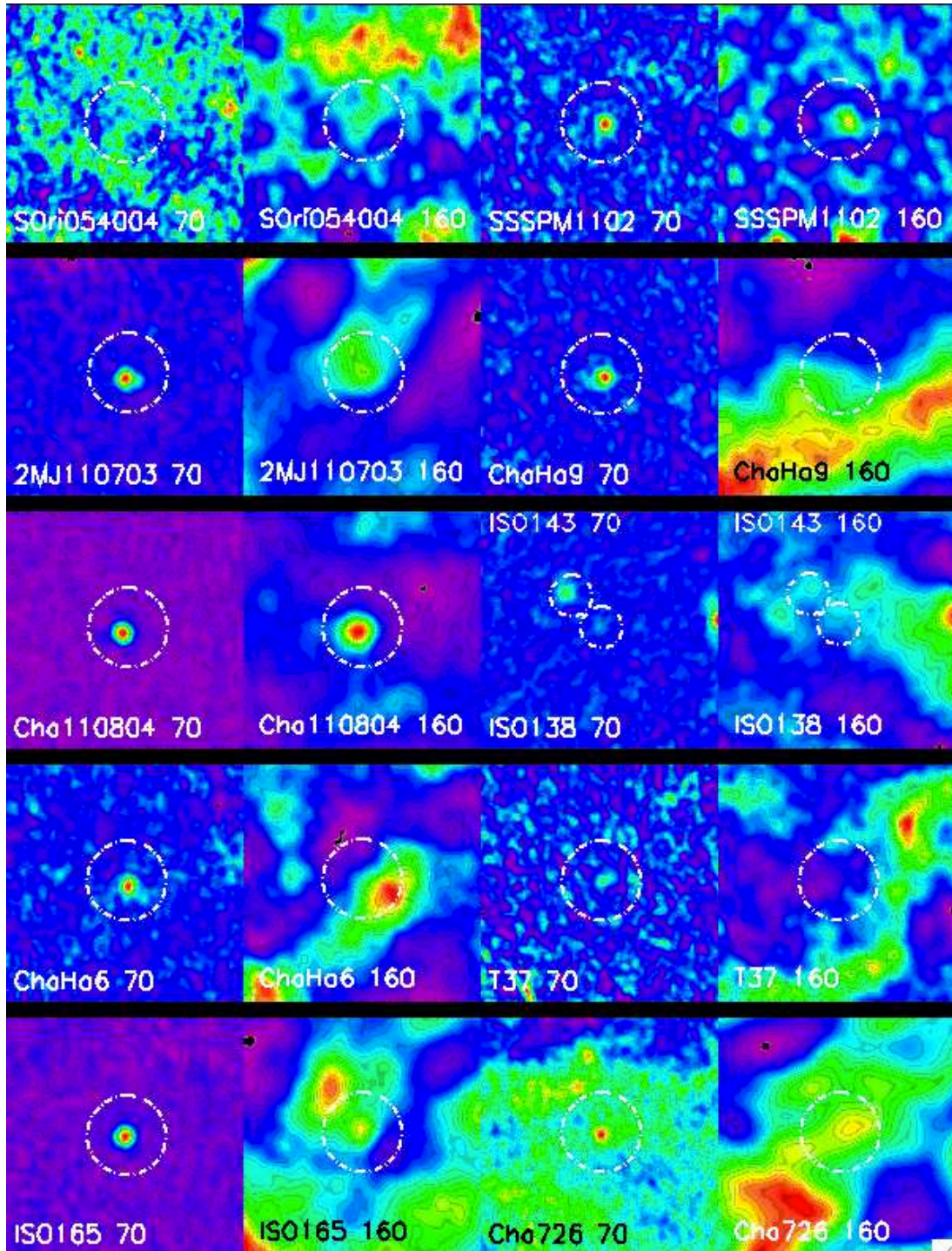


Fig. 4.— Images of next 11 objects in Table 3. Circle diameter for ISO138/143 is $16''$.

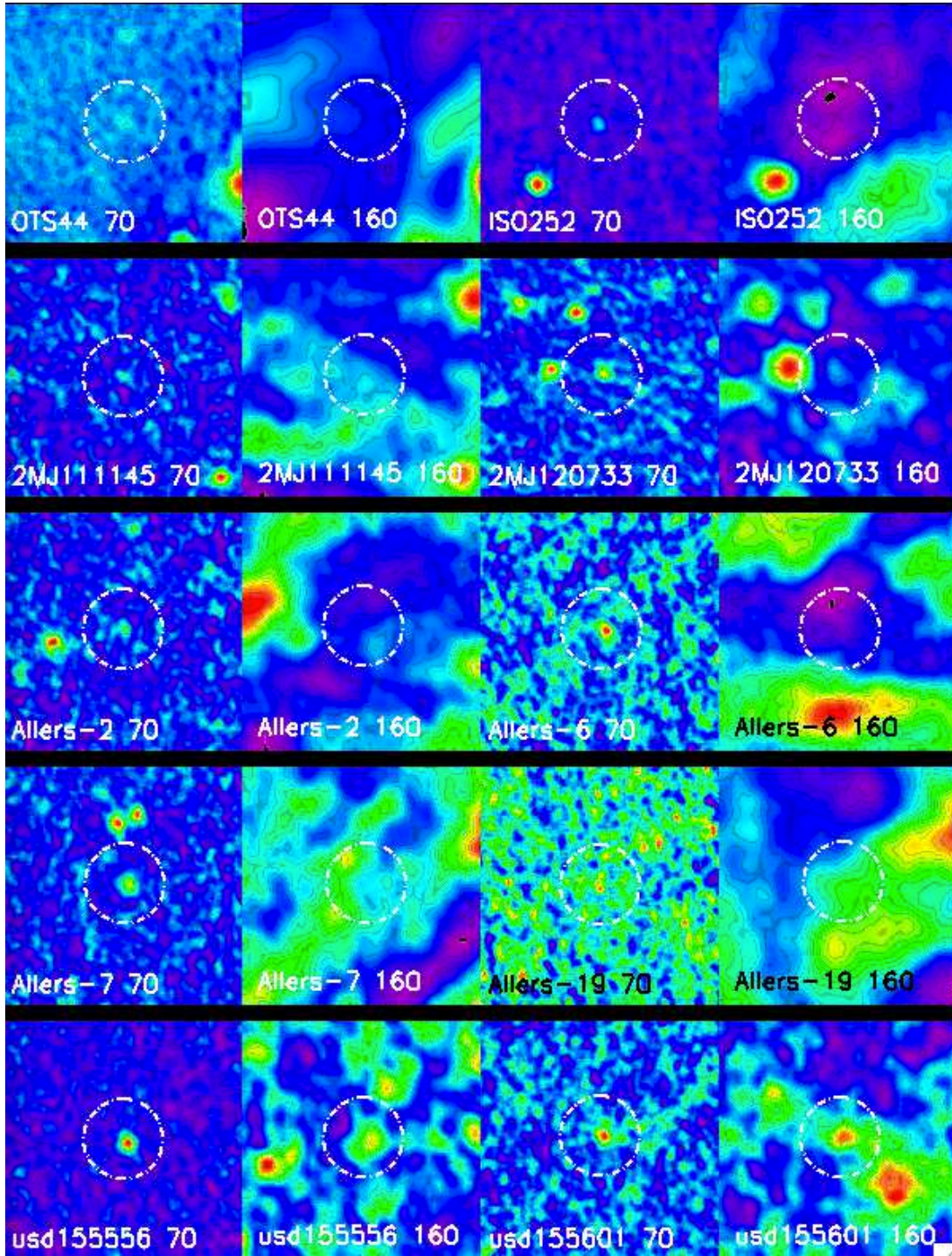


Fig. 5.— Images of next 10 objects in Table 3.

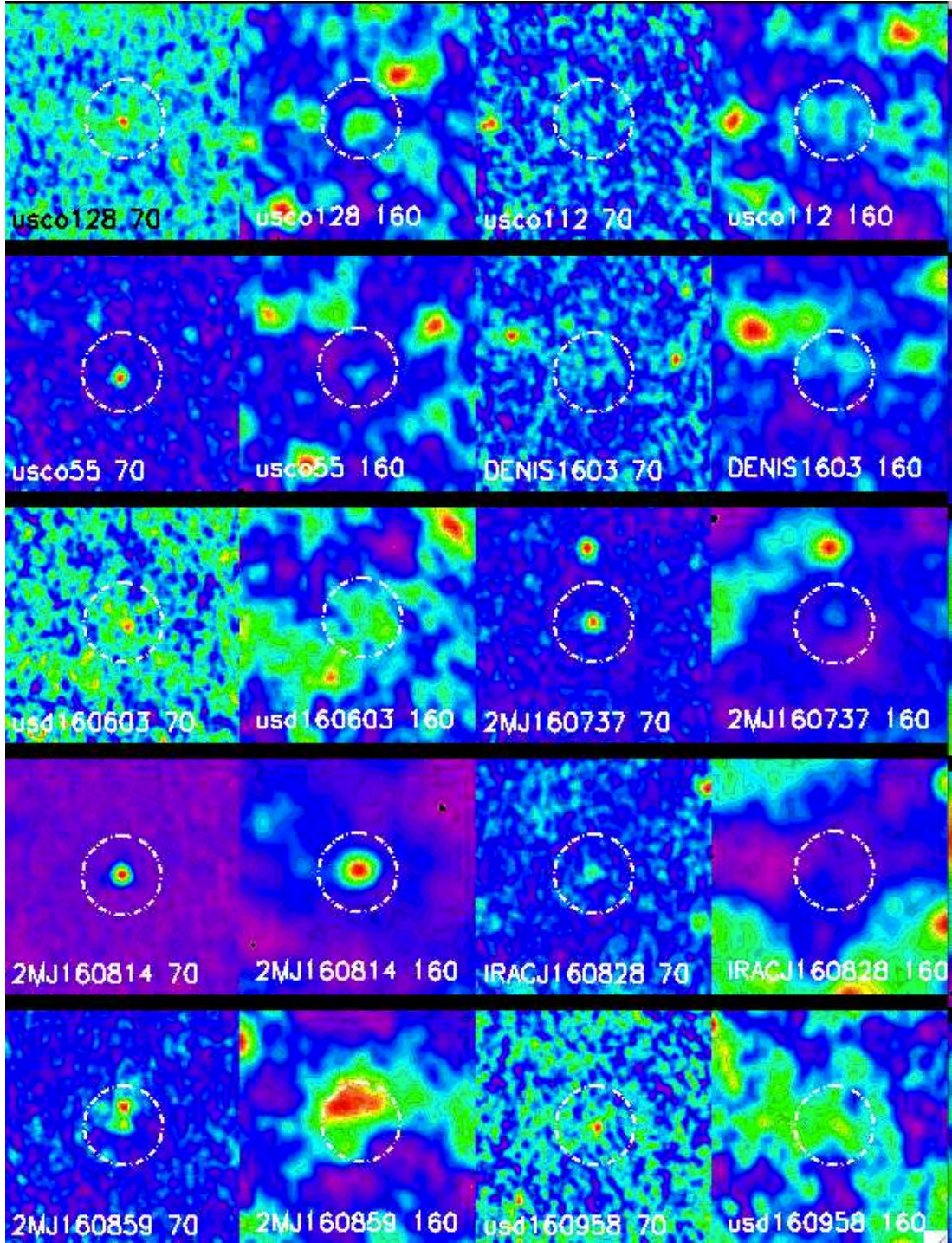


Fig. 6.— Images of next 10 objects in Table 3.

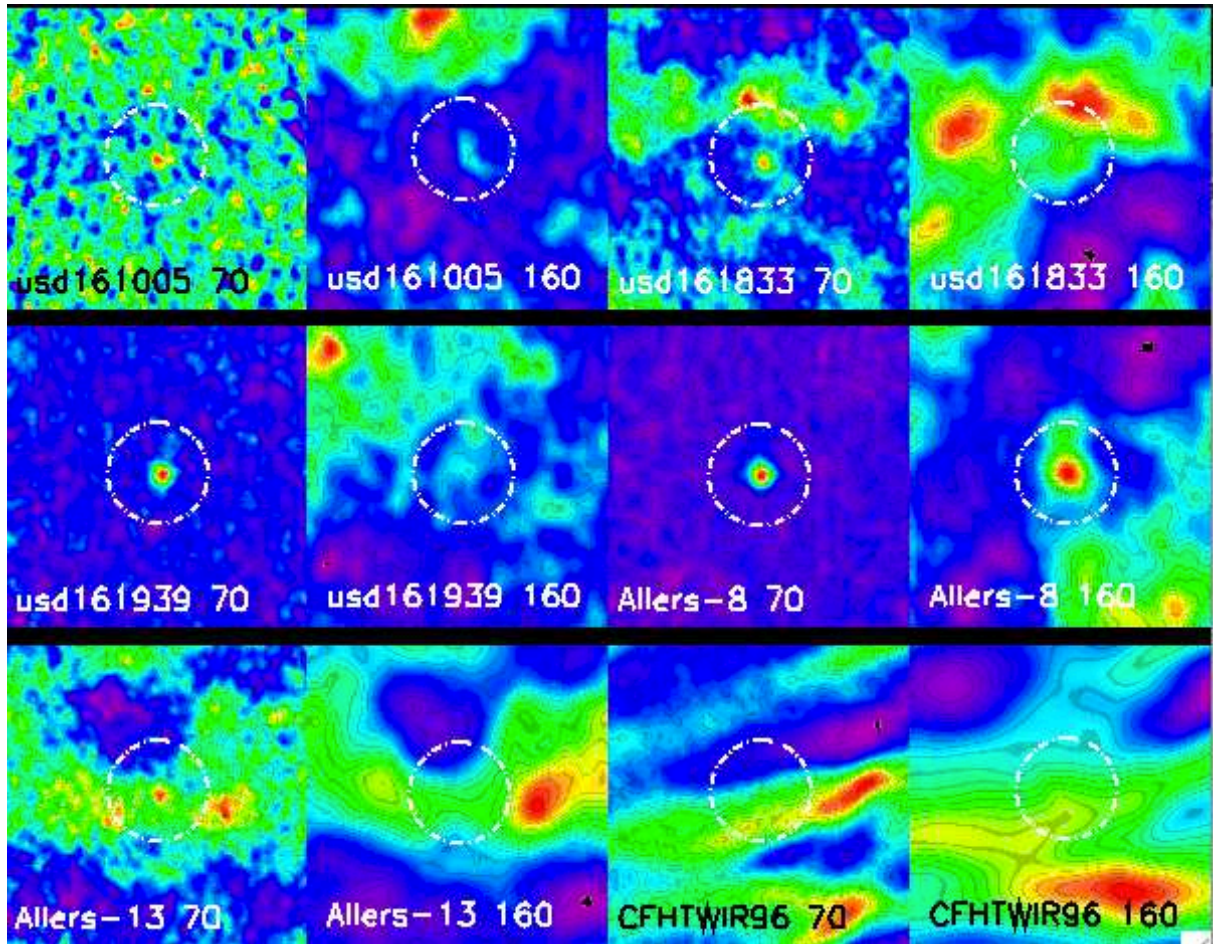


Fig. 7.— Images of last 6 objects in Table 3.

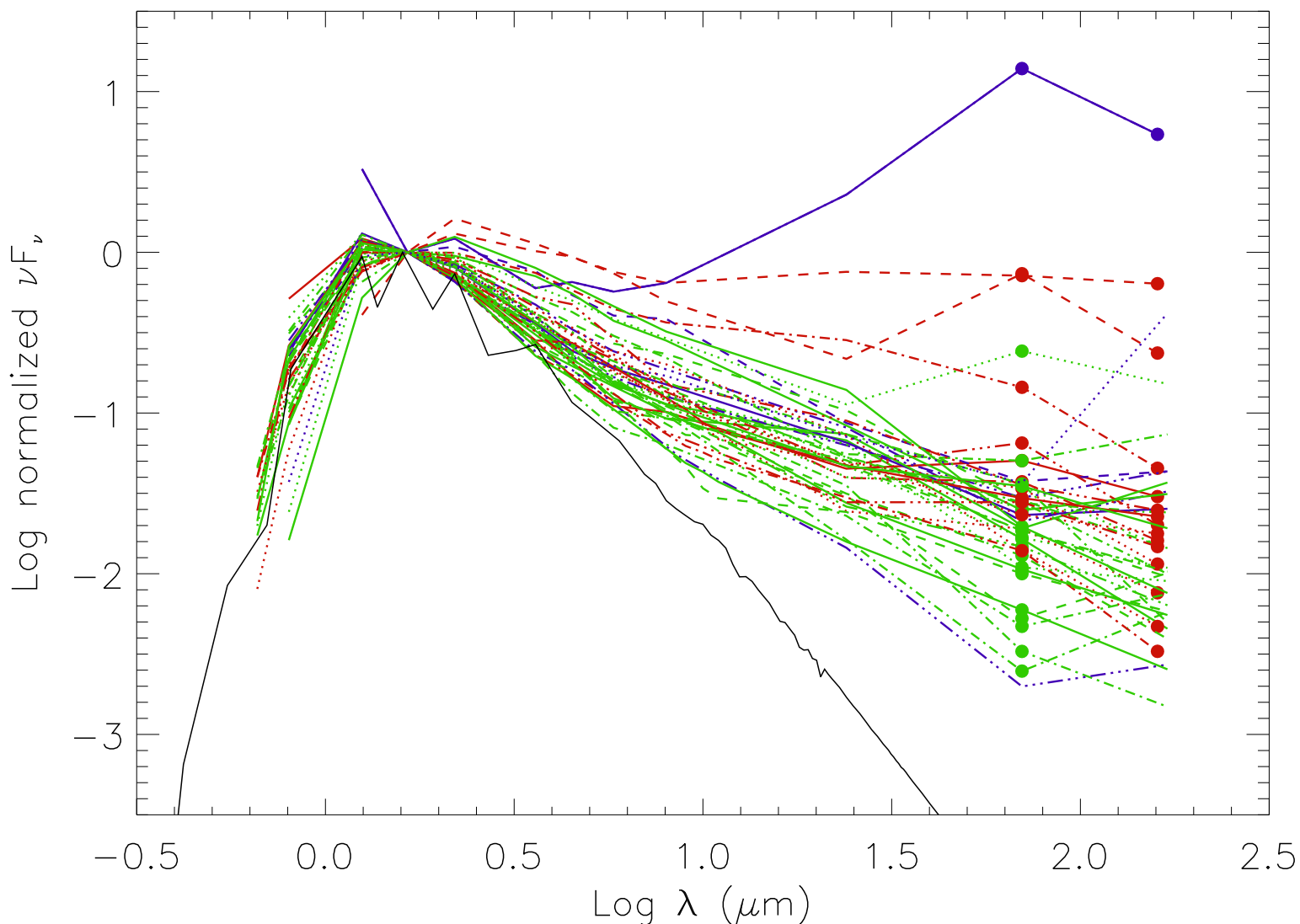


Fig. 8.— Overplotted SED’s normalized to $1.6\mu\text{m}$. Objects with $S/N > 2$ at both 70 and $160\mu\text{m}$ are shown with fluxes plotted as red circles and red SED’s. Objects with $S/N > 2$ only at $70\mu\text{m}$ are shown plotted in green, and remaining objects without reliable detections at either wavelength are in blue. Plotted fluxes without circles are only upper limits or low S/N . The solid black curve shows a typical SED of a bare BD photosphere (SSSPM110209 from Paper I). The possible Class I object, Cha110804, is the solid blue line with the highest values of normalized 70 and $160\mu\text{m}$ fluxes; note flux values for his object are upper limits shortward of $3.6\mu\text{m}$ as measured from the 2MASS survey images.

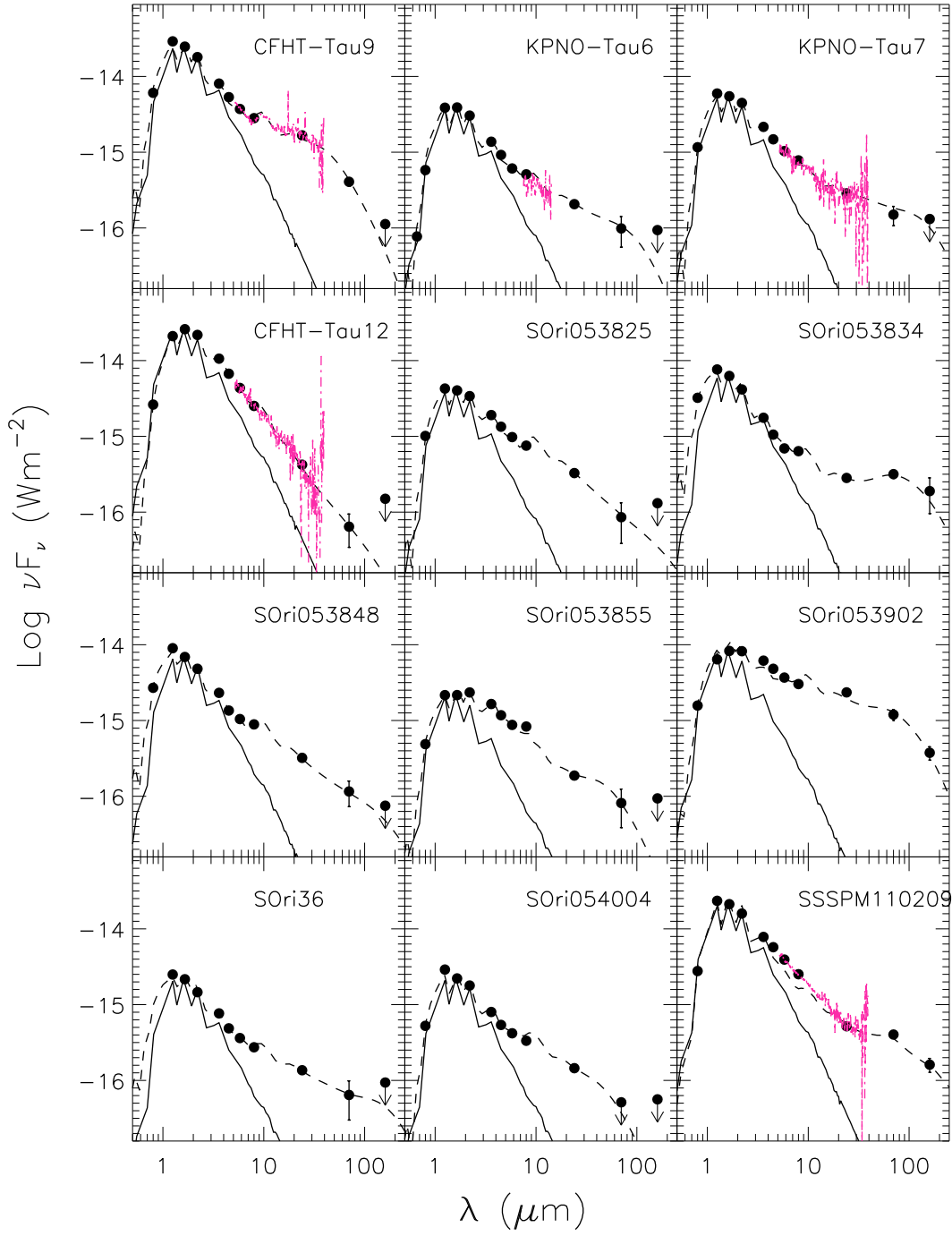


Fig. 9.— SED's of the first 12 Class II objects in Table 3. Representative model fits are shown with dashed lines, and Spitzer IRS data are shown in red. A typical bare photosphere is shown in solid, normalized to the observed $1.6\mu\text{m}$ flux.

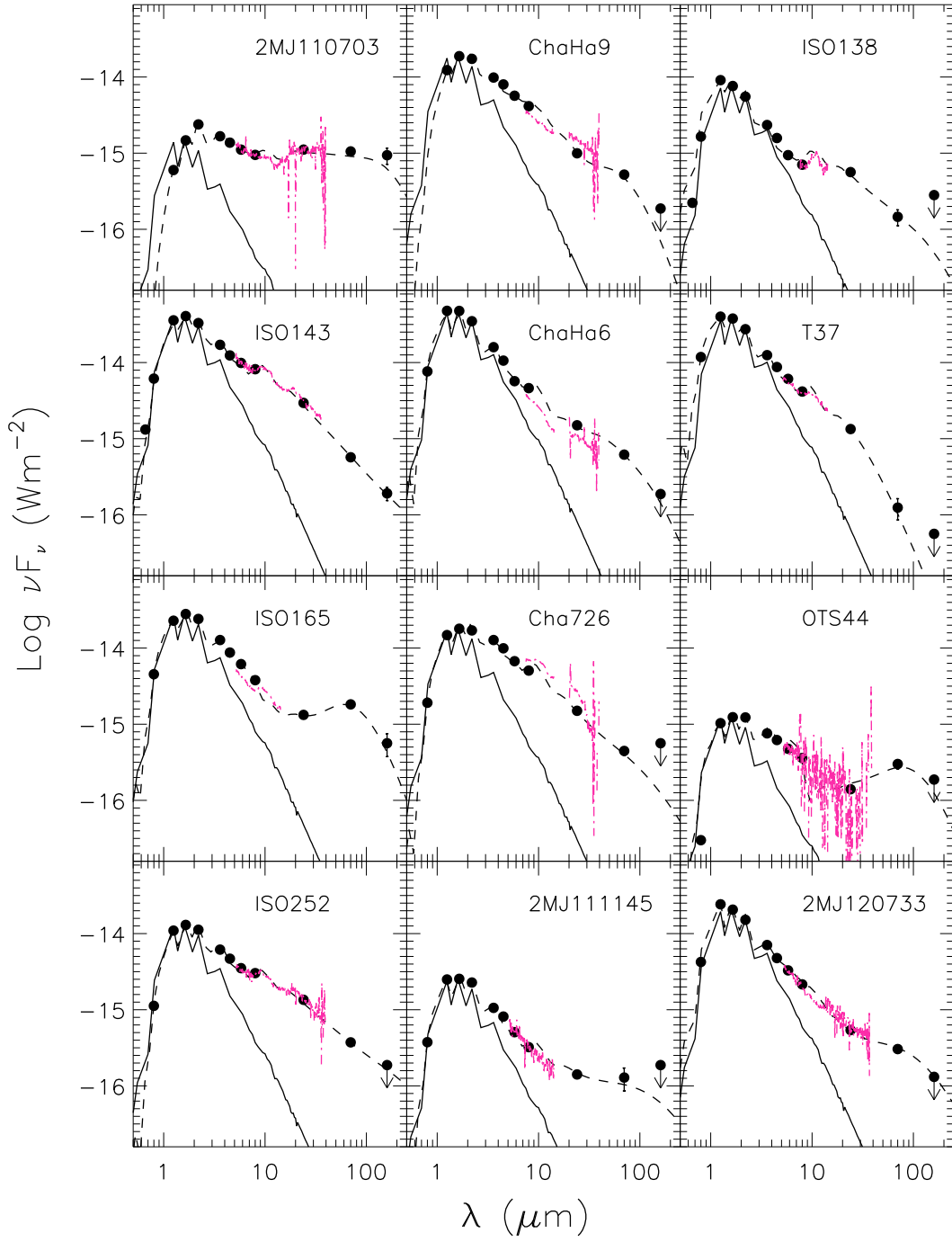


Fig. 10.— SED's of the second 12 Class II objects in Table 3.

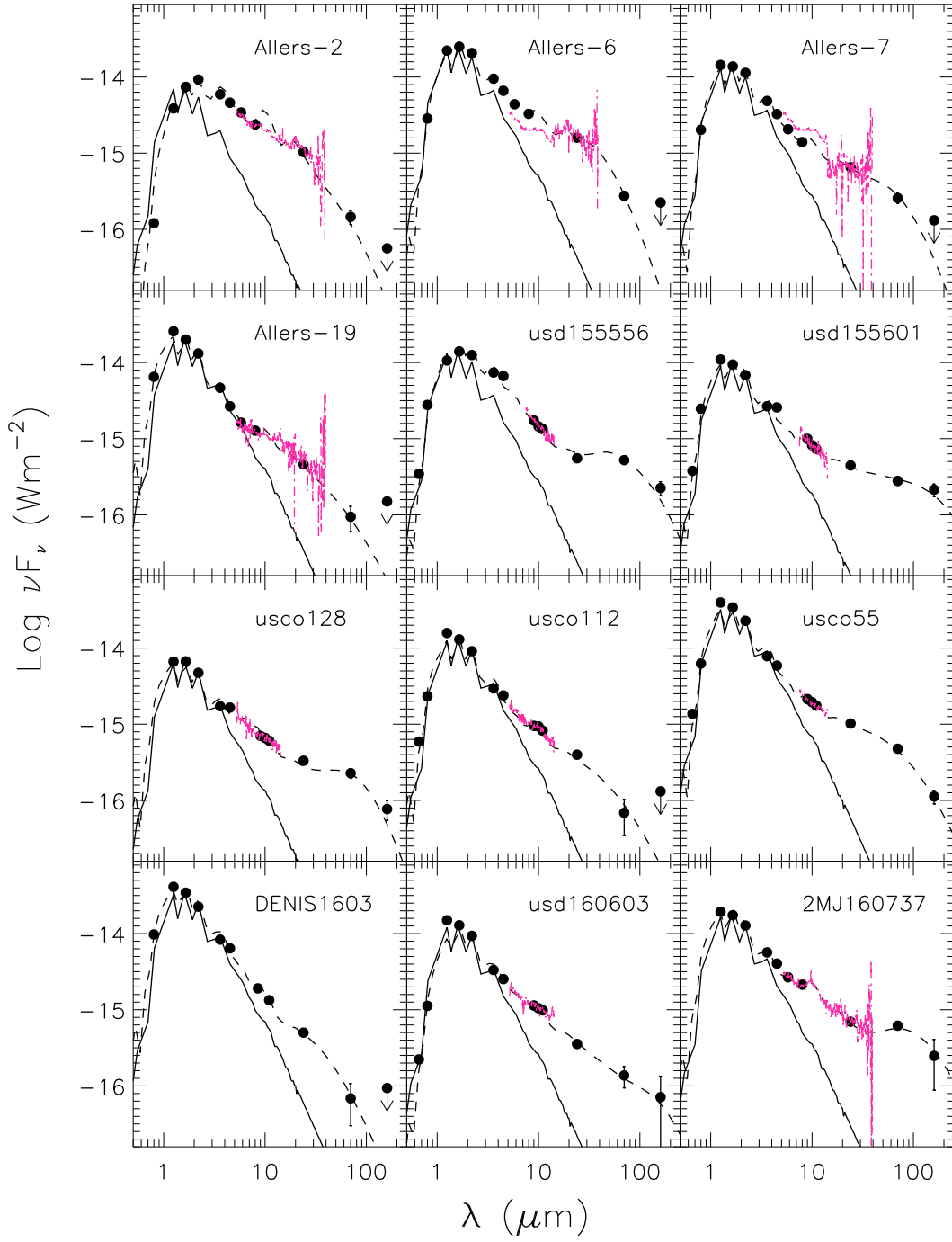


Fig. 11.— SED's of the third 12 Class II objects in Table 3.

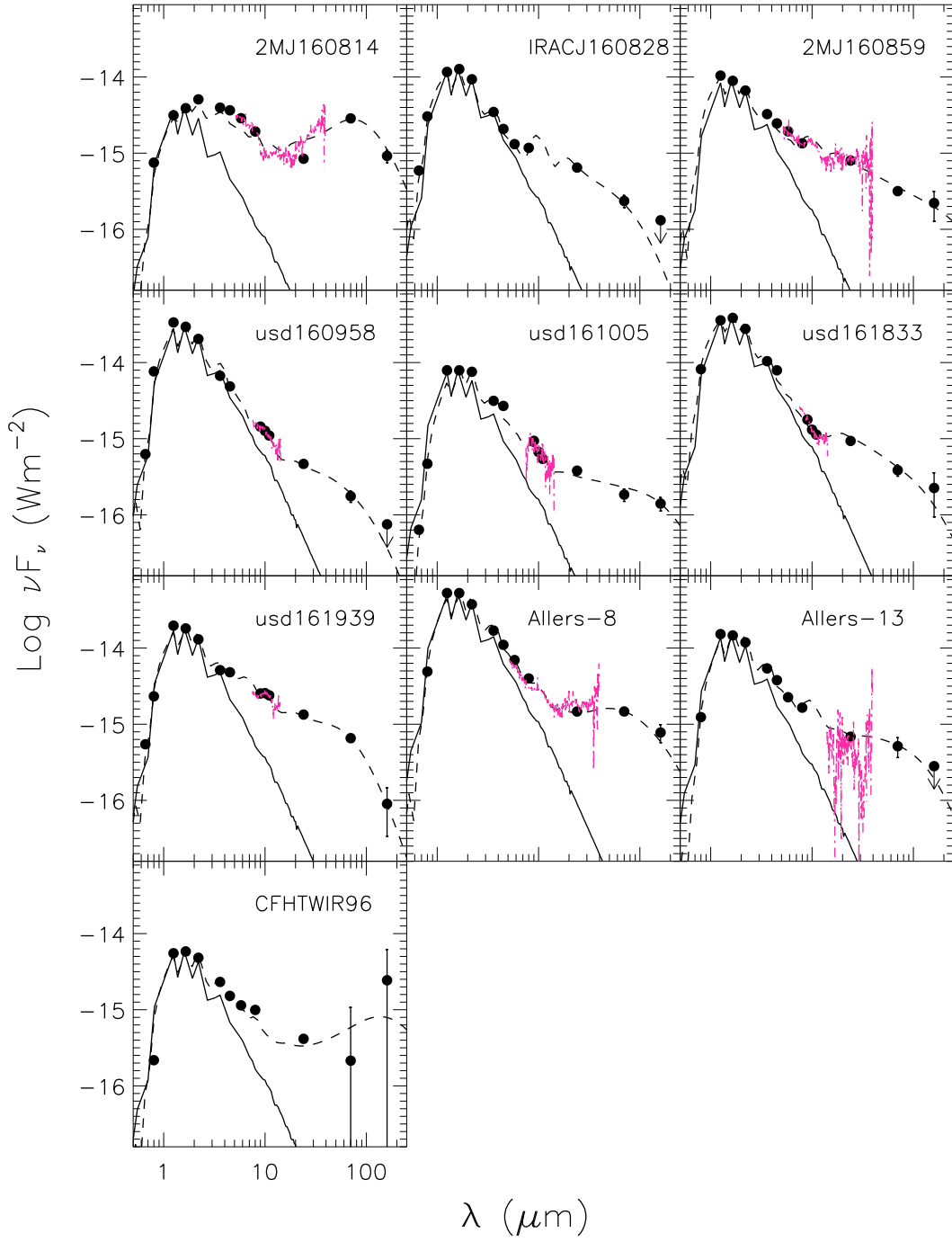


Fig. 12.— SED's of the last 10 Class II objects in Table 3.

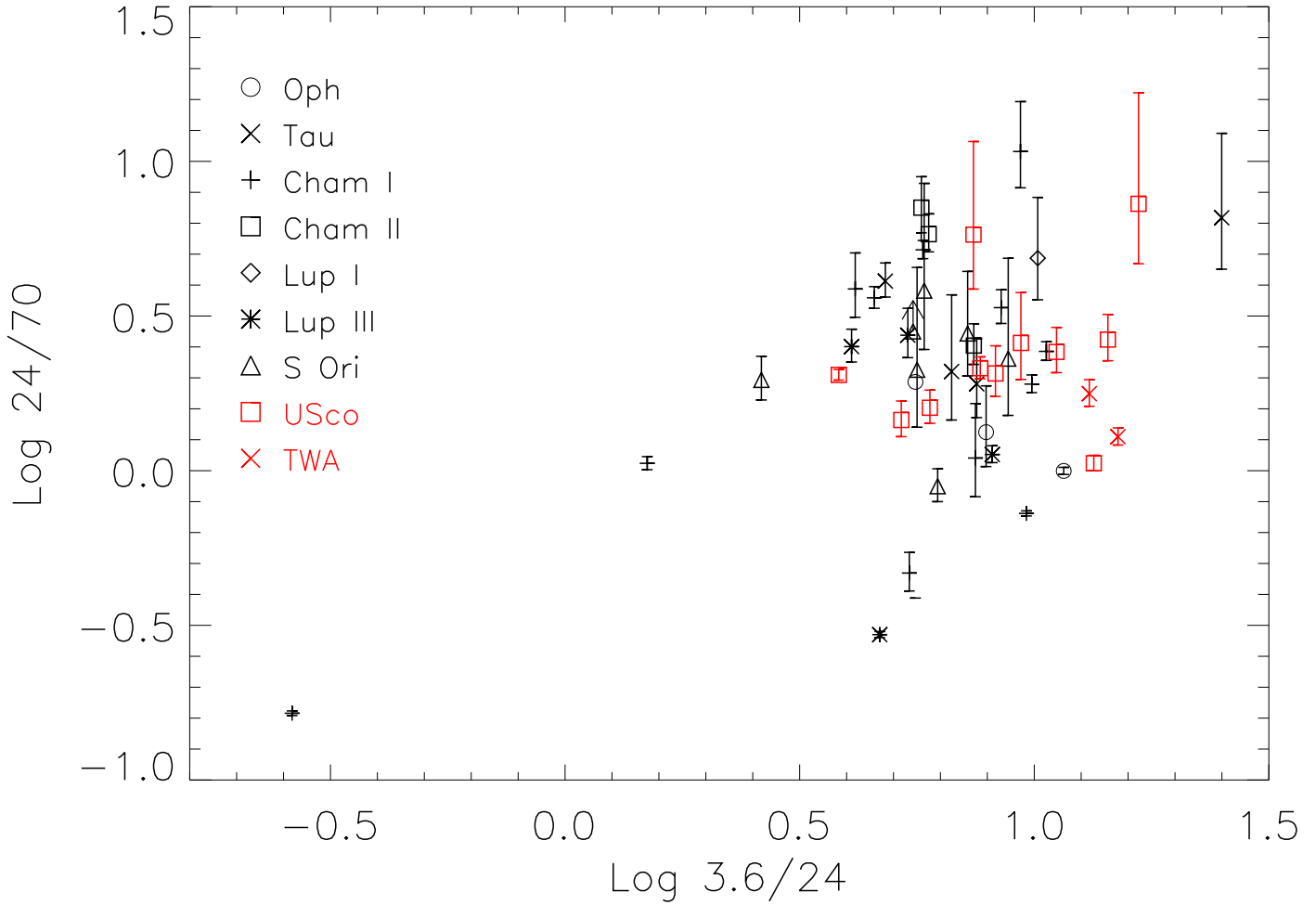


Fig. 13.— Color-color diagram showing far-ir color (νF_ν 24/70) versus mid-ir color (νF_ν 3.6/24) as a function of star-forming cloud in which the object is found. There is no clear trend with region, suggesting that there is no obvious dependence of outer disk structure/mass versus age.

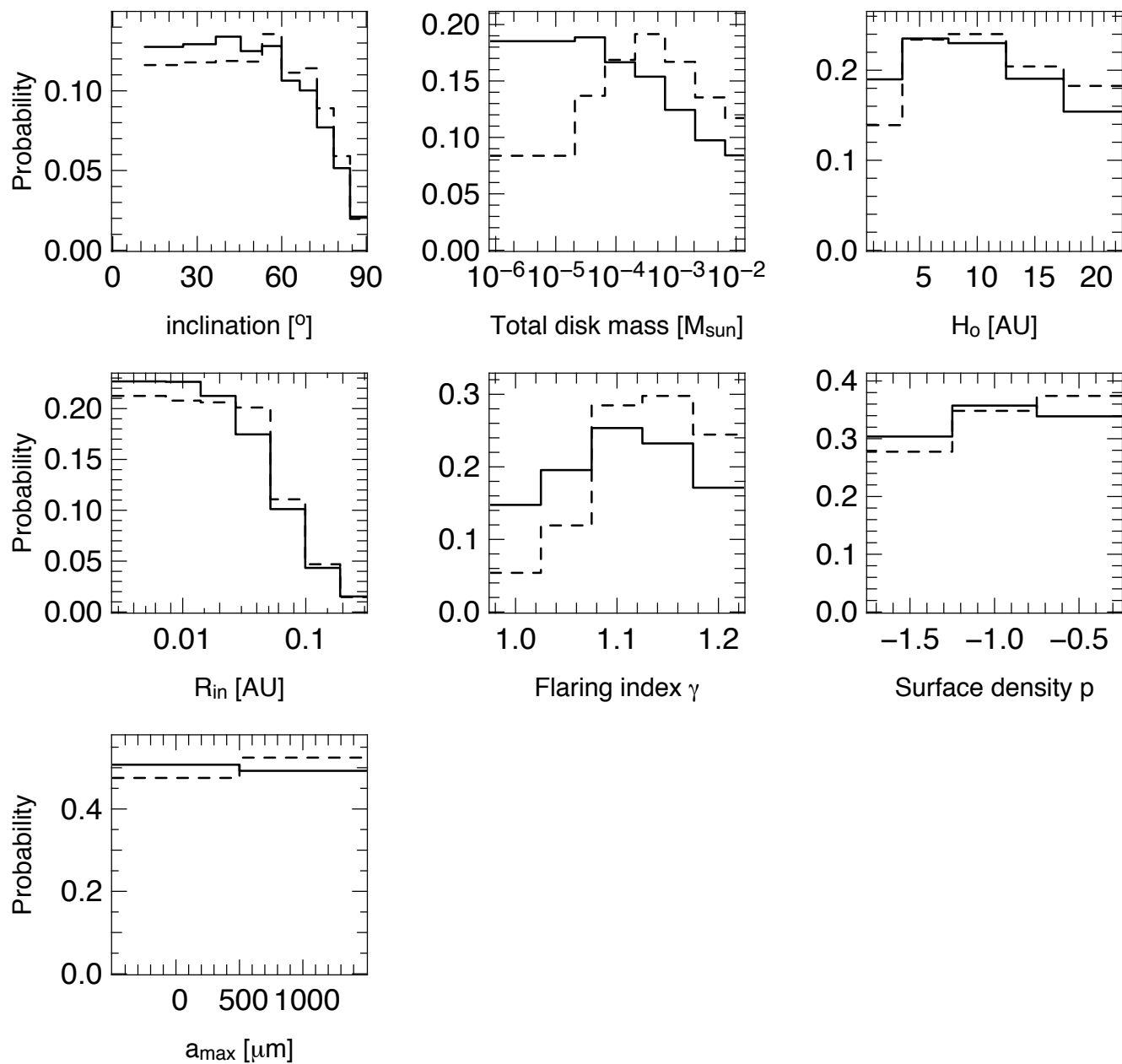


Fig. 14.— Histograms of the total of all probability distributions for the disk parameters illustrating the likely range of these parameters in the total sample. The solid line is for the entire sample and the dashed line is for just the objects detected at $160\mu\text{m}$.

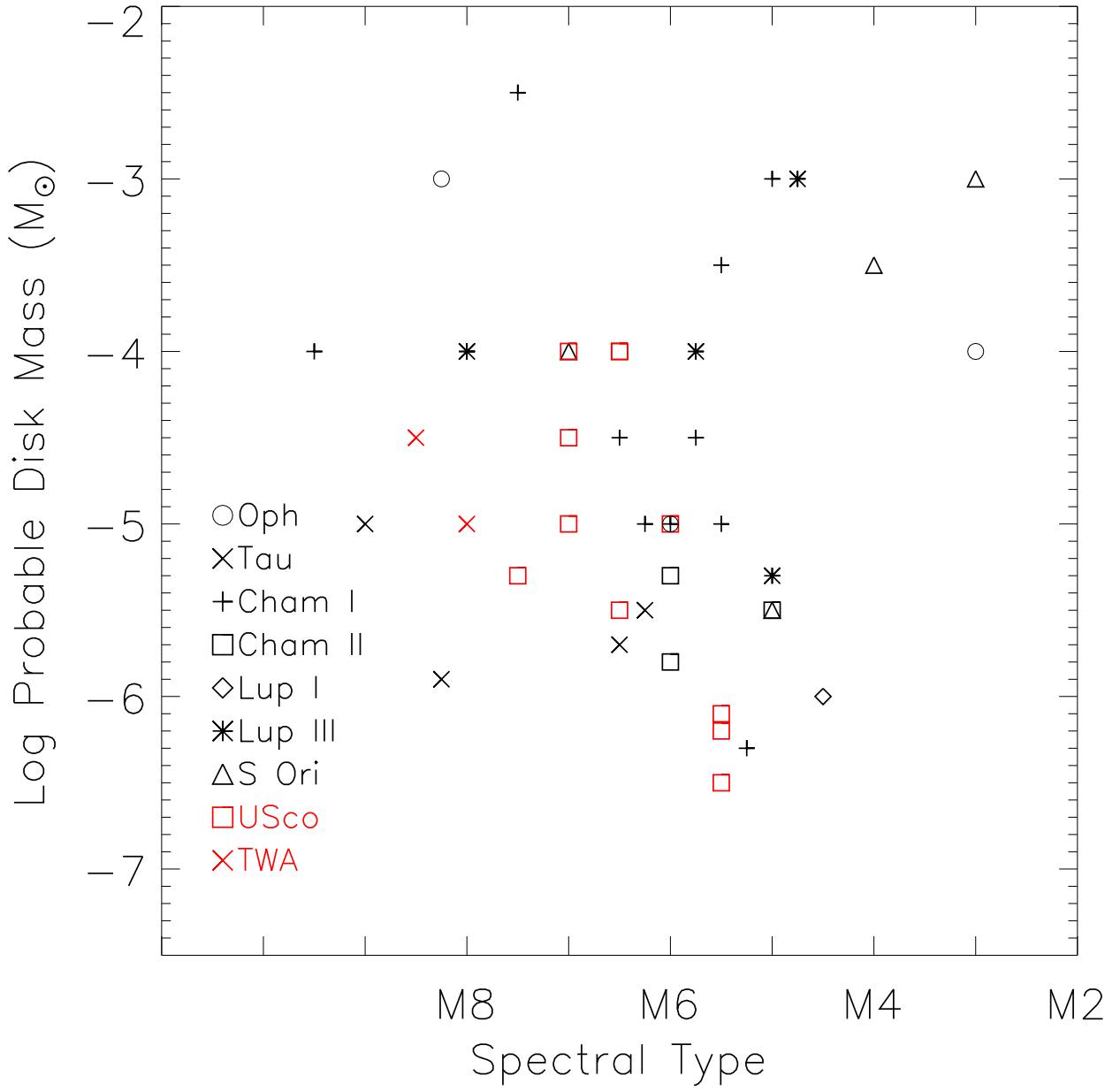


Fig. 15.— Most probable disk mass versus spectral type for the 43 objects with published spectral types.

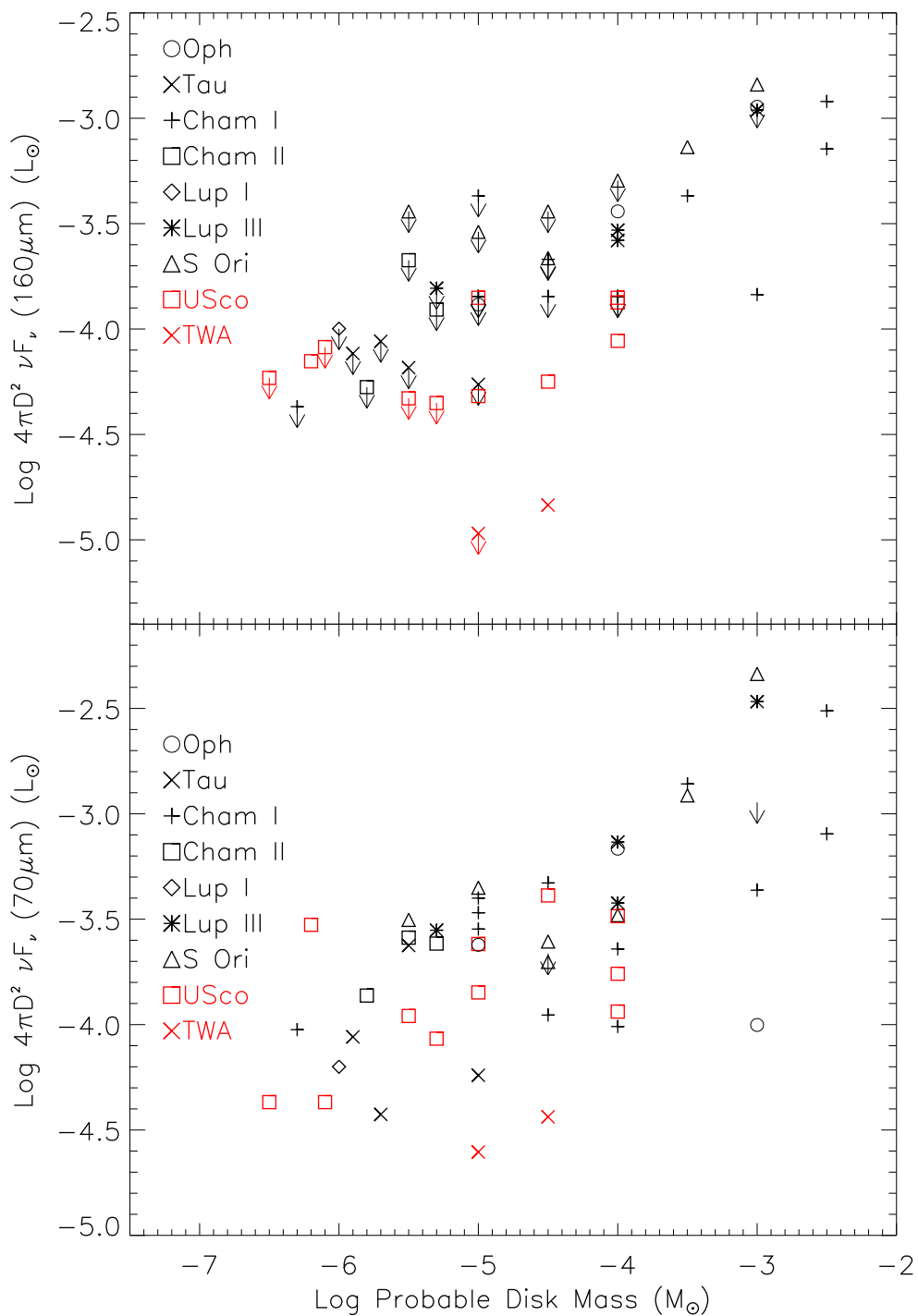


Fig. 16.— Comparison of the 70 and $160\mu\text{m}$ luminosities with the model-derived most probable disk masses illustrating the utility of the longest PACS wavelength for estimating disk masses.

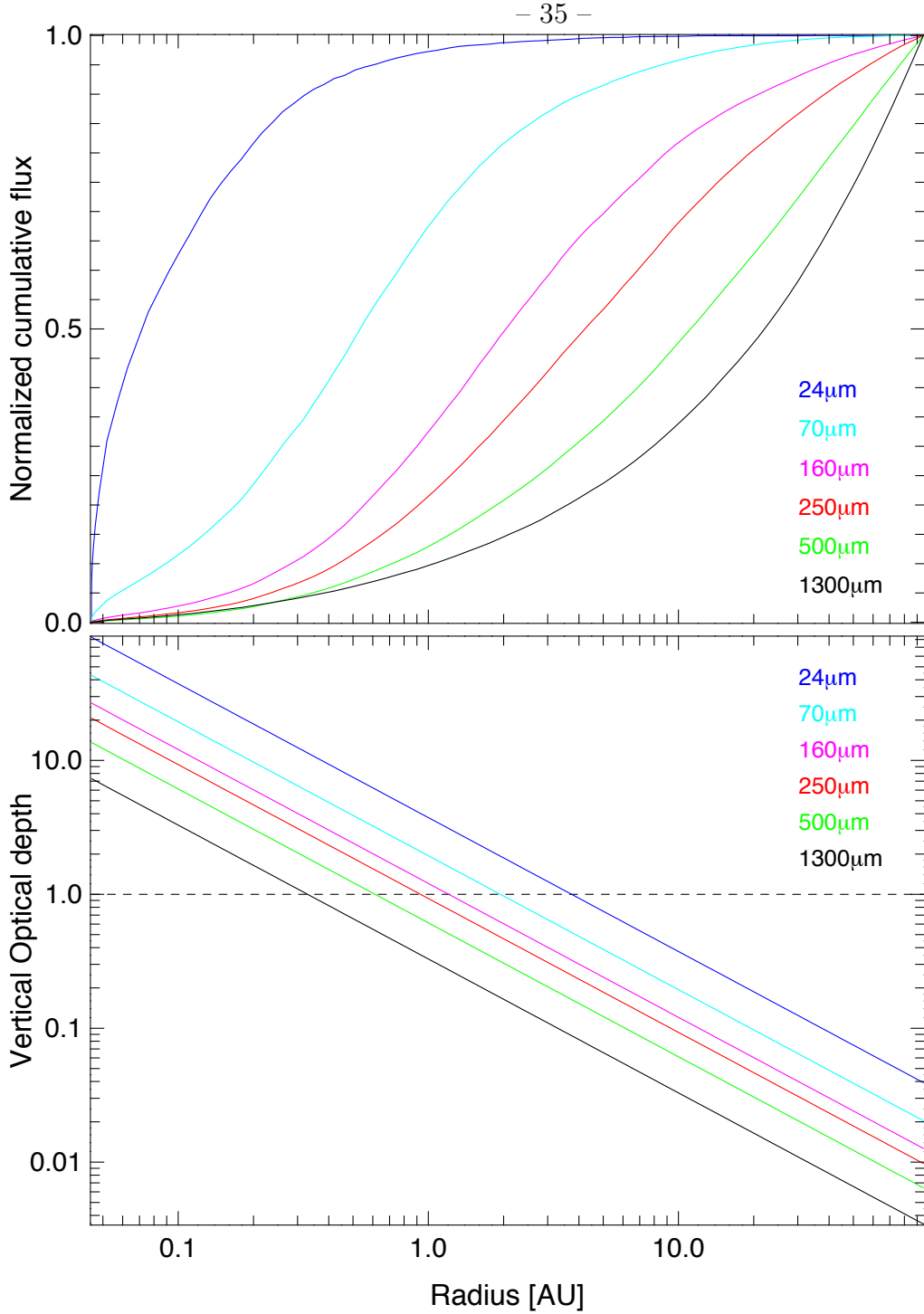


Fig. 17.— Upper panel – plot of cumulative emitted flux as a function of radius at several wavelengths for a typical disk model with $M_{disk} = 2 \times 10^{-4} M_{\odot}$, $R_{in} = 0.05$ AU, $a_{max} = 1$ mm, $i = 30^{\circ}$, and geometry equal to the likely values in Figure 14. Lower panel – optical depth perpendicular to the disk as a function of radius at the same wavelengths, illustrating that at $160\mu\text{m}$ and longer, the disks are typically optically thin over most of the radii emitting at those wavelengths.

REFERENCES

- Allard, F. & Hauschildt, P. H. 1995, *ApJ*, 441, 170
- Allen, P. R. et al. 2007, *ApJ*, 655, 1095
- Allers, K. N., Kessler-Silacci, J. E., Cieza, L. A. & Jaffe, D. T. 2006, *ApJ*, 644, 364
- Alves de Oliveira, C. et al. 2010, *A&A*, 515, A75
- André, P. et al. 2010, *A&A*, 518, L102
- Ardila, D., Martín, E. & Basri, G. 2000, *AJ*, 120, 479
- Biller, B., Allers, K., Liu, M., Close, L. M. & Dupuy, T. 2011, *ApJ*, 730, 39
- Bouy, H. et al. 2007, *A&A*, 463, 641
- Bouy, H. et al. 2008, *A&A*, 486, 877
- Caballero, J. A. et al. 2007, *A&A*, 470, 903
- Caballero, J. A. et al. 2008, *A&A*, 491, 515
- Cody, A. M. & Hillenbrand, L. A. 2011, *ApJ*, 741, 9
- Comerón, F. 2008, in *ASP Monograph Ser. 5, Handbook of Star Forming Regions, Vol. 2, The Southern Sky*, ed. B. Reipurth (San Francisco, CA: ASP), 295
- Comerón, F. 2011, *A&A*, 531, A33
- Comerón, F., Spezzi, L. & López Martí, B. 2009, *A&A*, 500, 1045
- Damjanov, I. et al. 2007, *ApJ*, 620, 1337
- Draine, B. T. 2003, *ApJ*, 598, 1017
- Evans, N. J., II et al. 2007, Final Delivery of Data From the c2d Legacy Project: IRAC and MIPS, http://data.spitzer.caltech.edu/popular/c2d/20071101_enhanced_v1/ Documents/c2d_del_document.pdf
- Gizis, J. E. 2002, *ApJ*, 575, 484
- Guieu, S. et al. 2007, *A&A*, 465, 855
- Gully-Santiago, M. A., Allers, K. N. & Jaffe, D. T. 2012, *Proc. Cool Stars 16*

- Harvey, P. M. et al. 2006, ApJ, 644, 307
- Harvey, P. M. et al. 2012, ApJ, 744, L1 (Paper I)
- Hauschildt, P. H., Allard, F. & Baron, E. 1999, ApJ, 512 377
- Hernandez, J. et al. 2007, ApJ, 662, 1067
- Kenyon, S. J., Gómez, M. & Whitney, B. A. 2008, in ASP Monograph Ser. 5, Handbook of Star Forming Regions, Vol. 2, The Southern Sky, ed. B. Reipurth (San Francisco, CA: ASP), 405
- Klein, R., Apai, D., Pascucci, I., Henning, Th., Waters, L. B. F. M. 2003, ApJ, 593L, 57
- Kraus, A. L., White, R. J. & Hillenbrand, L. A. 2005, ApJ, 633, 452
- López Martí, B., Eisloffel, J. & Mundt, R. 2005, A&A, 440, 139
- López Martí, B., Eisloffel, J., Scholz, A. & Mundt, R. 2005, A&A, 416, 555
- Luhman, K. L. 2004, ApJ, 602, 816
- Luhman, K. L. 2007, ApJS, 173, 104
- Luhman, K. L. et al. 2005, ApJ, 620, L51
- Luhman, K.L. et al. 2008, ApJ, 675, 1375
- Luhman, K.L. & Muench, A. A. 2008, ApJ, 684, 654
- Luhman, K.L. 2008, in ASP Monograph Ser. 5, Handbook of Star Forming Regions, Vol. 2, The Southern Sky, ed. B. Reipurth (San Francisco, CA: ASP), 169
- Luhman, K.L., Allen, P.R., Espaillat, C., Hartmann, L. & Calvet, N. 2010, ApJS, 186, 111
- Martín, E. L., Delfosse, X. & Guieu, S. 2004, AJ, 127, 449
- Mordasini, C., Alibert, Y., Benz, W., Klahr, H. & Henning, T. 2012, A&A, 541, 97
- Oloffson, J. et al. 2009, A&A, 507, 327
- Pecaut, M. J., Mamajek, E. E. & Bubar, E. J. 2012, ApJ, 746, 154
- Pilbratt, G. et al. 2010, A&A, 518, L1
- Pinte, C., Ménard, F., Duchêne & Bastien, P. 2006, A&A, 459, 797

- Pinte, C., et al. 2009, A&A, 498, 967
- Poglitsch, A. et al. 2010, A&A, 518, L9
- Rebull, L. et al. 2010, ApJS, 186, 259
- Riaz, B., Gizis, J. E. & Hmiel, A. 2006, ApJ, 639, L79
- Riaz, B. & Gizis, J. E. 2008, ApJ, 681, 1584
- Riaz, B. et al., 2012a, MNRAS, 420, 2603
- Riaz, B. et al., 2012b, MNRAS, 422, L6
- Riaz, B. et al., 2012c, MNRAS, in press
- Rigliaco, E. et al. 2011, A&A, 526, L6
- Schechter, P. L., Mateo, M., & Saha, A. 1993, PASP, 105, 1342
- Scholz, R.-D., McCaughrean, M. J., Zinnecker, H. & Lodieu, N. 2005, A&A, 430, L49
- Scholz, A., Jayawardhana, R. & Wood, K. 2006, ApJ, 645, 1498
- Scholz, A. et al. 2007, ApJ, 660, 1517
- Skrutskie, M. et al. 2006, AJ, 131, 1163
- Szücs, L. et al., 2010, ApJ, 720, 1668
- Walker, C. et al. 2004, MNRAS, 351, 607
- Webb, R. A. et al. 1999, ApJ, 512, L63
- Werner, M. W. et al. 2004, ApJS, 154, 1
- Williams, J. P. & Cieza, L. A. 2011, Ann. Rev. Astr. Ap., 49, 67
- Wolf, S., Henning, Th. & Stecklum, B. 1999, A&A, 349, 839
- Wolf, S. 2003, ApJ, 582, 859
- Wright, E. L. 2010, AJ 140, 1868

